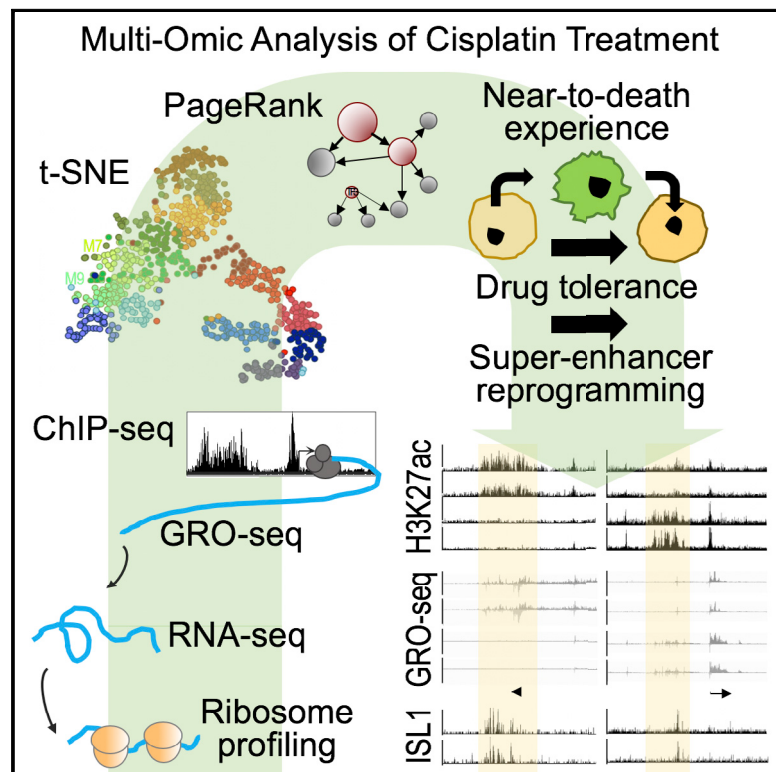


Super-Enhancer Redistribution as a Mechanism of Broad Gene Dysregulation in Repeatedly Drug-Treated Cancer Cells

Graphical Abstract



Authors

Qi Ma, Feng Yang, Carlos Mackintosh, ..., Dong Wang, Angels Almenar-Queralt, Ivan Garcia-Bassets

Correspondence

ibassets@health.ucsd.edu

In Brief

Ovarian tumors acquire new phenotypic features when exposed to anticancer therapy, which helps them endure the struggle for survival and increase malignancy. Using a six-layered multiomic approach, Ma et al. find that selective super-enhancer redistribution is a major driver of the acquisition of new phenotypic features.

Highlights

- A 6-layered multiomic approach provides an integrated view of cisplatin treatment
- Repeated cisplatin treatment leads to selective super-enhancer (SE) redistribution
- The most cisplatin-dysregulated genes locate nearby redistributed SE regions
- ISL1 is a SE regulator suppressed when cells struggle with cisplatin treatment



Super-Enhancer Redistribution as a Mechanism of Broad Gene Dysregulation in Repeatedly Drug-Treated Cancer Cells

Qi Ma,¹ Feng Yang,^{1,4} Carlos Mackintosh,^{1,4} Ranveer Singh Jayani,¹ Soohwan Oh,¹ Chunyu Jin,¹ Sreejith Janardhanan Nair,¹ Daria Merkurjev,¹ Wubin Ma,¹ Stephanie Allen,¹ Dong Wang,² Angels Almenar-Queralt,³ and Ivan Garcia-Bassets^{1,5,*}

¹Department of Medicine, School of Medicine, University of California, San Diego, La Jolla, CA 92093, USA

²School of Basic Medical Sciences, Chengdu University of Traditional Chinese Medicine, Chengdu, Sichuan 611137, China

³Department of Cellular and Molecular Medicine, University of California, San Diego, La Jolla, CA 92093, USA

⁴These authors contributed equally

⁵Lead Contact

*Correspondence: ibassets@health.ucsd.edu

<https://doi.org/10.1016/j.celrep.2020.107532>

SUMMARY

Cisplatin is an antineoplastic drug administered at suboptimal and intermittent doses to avoid life-threatening effects. Although this regimen shortly improves symptoms in the short term, it also leads to more malignant disease in the long term. We describe a multilayered analysis ranging from chromatin to translation—integrating chromatin immunoprecipitation sequencing (ChIP-seq), global run-on sequencing (GRO-seq), RNA sequencing (RNA-seq), and ribosome profiling—to understand how cisplatin confers (pre)malignant features by using a well-established ovarian cancer model of cisplatin exposure. This approach allows us to segregate the human transcriptome into gene modules representing distinct regulatory principles and to characterize that the most cisplatin-disrupted modules are associated with underlying events of super-enhancer plasticity. These events arise when cancer cells initiate without ultimately ending the program of drug-stimulated death. Using a PageRank-based algorithm, we predict super-enhancer regulator ISL1 as a driver of this plasticity and validate this prediction by using CRISPR/dCas9-KRAB inhibition (CRISPRi) and CRISPR/dCas9-VP64 activation (CRISPRa) tools. Together, we propose that cisplatin reprograms cancer cells when inducing them to undergo near-to-death experiences.

INTRODUCTION

Cisplatin is a widely used anticancer drug that forms cisplatin-DNA adducts that can obstruct DNA synthesis and transcription (Damia and Broggini, 2019). Cisplatin can also interact with RNA and proteins, which can be highly disruptive to cells (Raudenska et al., 2019). These pleiotropic effects halt cell division, and arrested cells engage in a program of cell death if the number of

cellular disturbances reaches a certain threshold (Damia and Broggini, 2019; Raudenska et al., 2019). Cisplatin is the standard first-line therapy against cancer types such as ovarian cancer. In most ovarian cancer patients, the drug improves symptoms in the short term, but it is ineffective in the long term (Holohan et al., 2013; Mansoori et al., 2017). Arguably, cisplatin ultimately fails because it is administered at sublethal and intermittent doses to manage the narrow range of drug doses that generate a therapeutic response without causing adverse effects intolerable for patients. This regimen facilitates the survival of intrinsically resilient cells, and—worse—it allows them to adopt transcriptomic features that help them endure the struggle for survival and increase malignancy over time (Bradner et al., 2017; Easwaran et al., 2014; Flavahan et al., 2017; Knoechel et al., 2014; Koppikar et al., 2012; Liau et al., 2017; Roesch et al., 2013; Shaffer et al., 2017; Sharma et al., 2010).

Transcriptomic reprogramming is a well-established feature induced by repeated cisplatin exposure, but the driving mechanisms remain relatively unknown (Andorfer et al., 2016; Lloyd et al., 2015; Shen et al., 2012). These mechanisms are likely complex due to the multilayered actions of cisplatin on DNA, RNA, and proteins at the same time. To characterize these mechanisms, therefore, we postulated that it would be instrumental to first segregate the human transcriptome into modules in which each module represents a subset of genes that share a multilayered regulatory principle. Here, we segregated the coding transcriptome of A2780 cells into modules. A2780 cells represent one of the most popular models in the field of ovarian cancer established from a now-considered endometrioid-type ovarian tumor (Anglesio et al., 2013; Beaufort et al., 2014; Domcke et al., 2013; Ince et al., 2015). A2780 cells are known to undergo transcriptomic reprogramming after repeated cisplatin treatment (Helleman et al., 2006; Li et al., 2009; Solár and Sytkowski, 2011; Verhaak et al., 2013; Zeller et al., 2012). To annotate and segregate gene modules that share multilayered regulatory principles, first, we profiled the three major RNA processing steps—RNA synthesis, accumulation, and translation—under different cisplatin treatment conditions in these cells. Then, we applied an analytical strategy known as Seurat that identifies patterns of expression variation in multidimensional data.



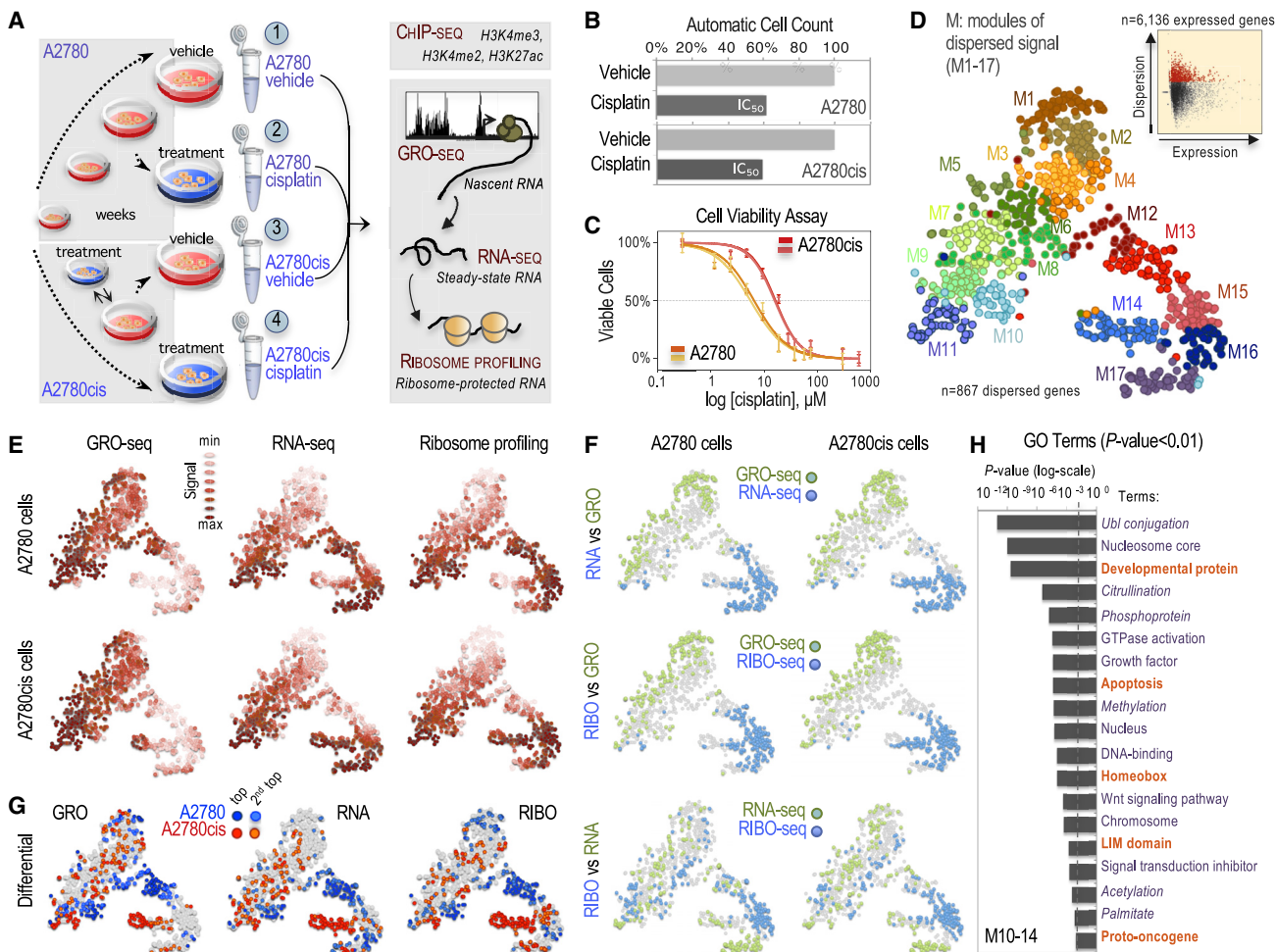


Figure 1. Multidimensional Analysis of the A2780 Model after Cisplatin Treatment

(A) Experimental workflow. See text.

(B) Automated cell count analysis based on trypan-blue staining after cisplatin exposure of 2 and 6 μM in A2780 and A2780cis cells for 3 days, respectively (format: 15-cm culturing plates). Error bars represent standard deviation of the mean of $n = 3$ technical replicates.

(C) Dose-response curve of 2-day cisplatin exposure in A2780 and A2780cis cells (format: 96-well culturing plates). Each line represents an independent experiment ($n = 2$). Error bars represent standard deviation of the mean of three technical replicates in each experiment ($n = 3$).

(D) t-SNE plot represents the expression admixture ($n = 12$ measurements; see A) for the $n = 867$ genes with the highest signal dispersion after integrating GRO-seq, RNA-seq, and ribosome-profiling data of 3-day vehicle- and cisplatin-treated A2780 and A2780cis cells and segregated in $n = 17$ color-coded modules (M1-17) identified by K-means. Graph represents dispersion (MeanVarPlot) of the $n = 6,136$ genes (out of $n = 19,197$ coding transcripts) that reach the threshold of detection in at least one of the 12 measurements. The red dots represent the $n = 867$ most dispersed genes. The x axis represents log-scaled variance to mean ratio (VMR). The y axis represents normalized average (mean) expression. See also Figure S1D.

(E-G) Distribution of normalized signal (vehicle condition) across the t-SNE plot shown in (D) by assays in (E) (colors represent 9 ranks of signal: from minimum to maximum), by differential signal comparing assays in (F) (colors represent the top two ranks out of nine of differential signal between assays), and by differential signal comparing A2780 and A2780cis in (G) (colors represent the top two ranks out of nine of differential signal between A2780 and A2780cis cells). See Figure S1E-S1G for 3-day cisplatin treatment.

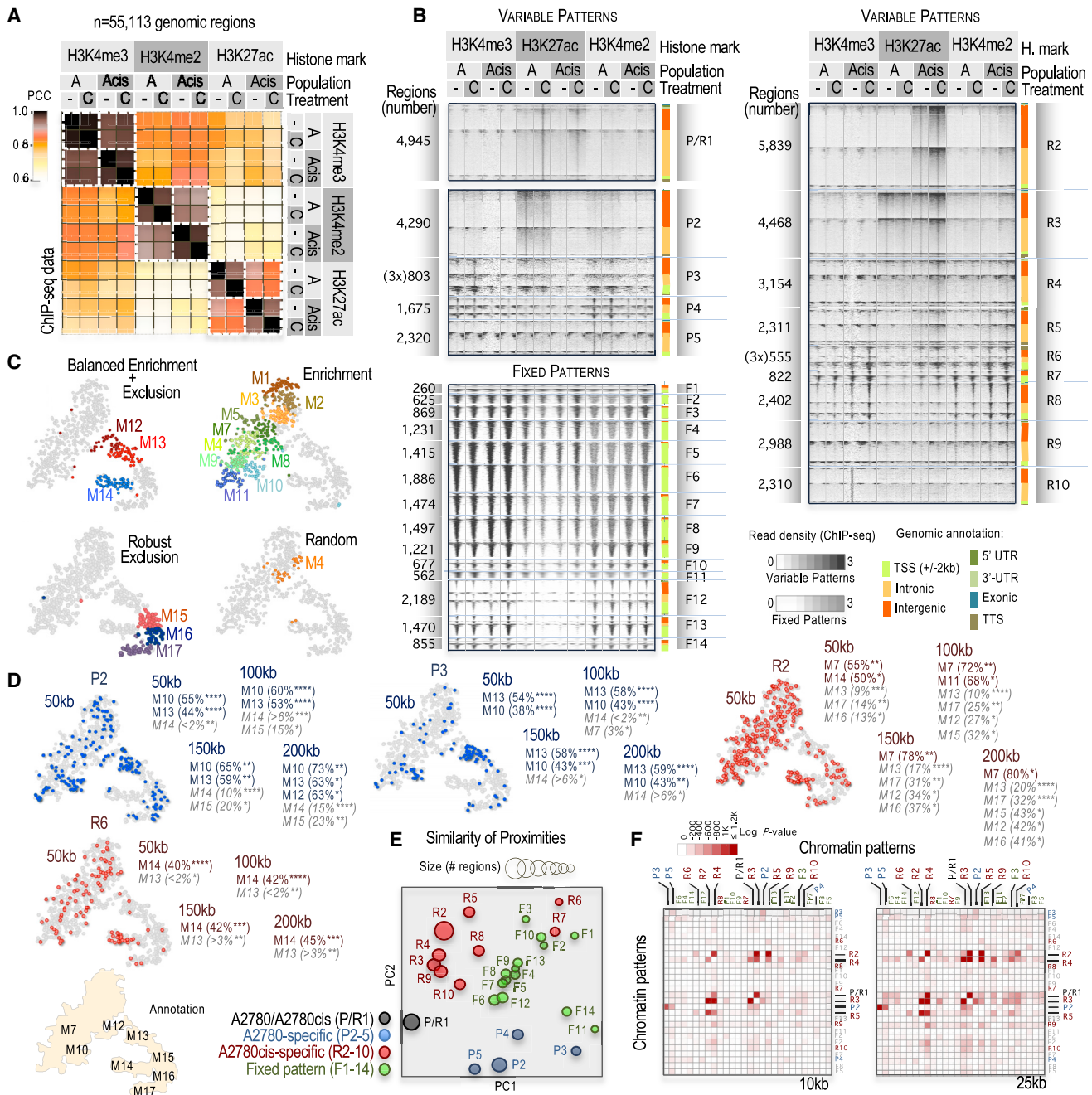
(H) GO analysis of the $n = 256$ genes in the M10-14 modules. Selected terms with $p < 0.01$. See Figure S1H for GO analysis module by module. See also Figure S1 and Table S1.

RESULTS

Modular Segregation of the A2780 Coding Transcriptome

We used global run-on sequencing (GRO-seq) to profile RNA synthesis, RNA sequencing (RNA-seq) to profile RNA accumulation, and ribosome profiling as a proxy to profile translation in short tan-

dem repeat (STR)-authenticated A2780 cells and in repeatedly pretreated A2780 cells (A2780cis) in the absence or the presence of cisplatin concentrations that cause 50% loss in cell viability (IC₅₀) after a 3-day treatment (Figures 1A, 1B, S1A, and S1B). Pretreated A2780cis cells are more tolerant to cisplatin than A2780 cells (Figure 1C), as expected, but applying an equivalent IC₅₀ dose leads to the upregulation of well-known cisplatin-stimulated transcripts in

**Figure 2. Multilayered Chromatin Analysis of the A2780 Model after Cisplatin Treatment**

- (A) Similarity matrix analysis (Pearson correlation coefficient [PCC]) of H3K4me3, H3K4me2, and H3K27ac ChIP-seq profiles in 3-day cisplatin-treated and untreated A2780/A2780cis cells (see Figure 1A). Analysis of the n = 55,113 histone-mark-enriched regions in at least one condition/population. -/C, vehicle/cisplatin; A/Acis, A2780/A2780cis cells.
- (B) Patterns of chromatin organization determined by K-means (Pearson) based on read density distribution across 6-kb windows centered at the peak of each of the n = 55,113 histone-mark-enriched regions. Regions sorted by functional annotation (indicated on the side). 3x indicates the panel is 3-fold enlarged for visualization purposes.
- (C) Summary of enrichment and exclusion of chromatin patterns (χ^2 , $p \leq 10^{-3}$) from the TSS of dispersed genes (range, 200 kb) segregated by modules. See statistics in Figure S2G, 200 kb panel.
- (D) Dispersed genes (in blue or red) within 50 kb of the indicated chromatin pattern. Modules with higher (in blue or red) or lower (in gray italic font) number of genes than randomly expected (χ^2 , $p \leq 10^{-3}$) are indicated at different distances (50, 100, 150, and 200 kb), as well as the percentage of cases over the total of genes in the module, and the P-value of "enrichment" or "exclusion and scarcity." t-SNE plot with annotations was used as reference. * $p \leq 10^{-3}$, ** $p \leq 10^{-4}$, *** $p \leq 10^{-5}$, **** $p \leq 10^{-6}$.

(legend continued on next page)

both cell populations (6 and 2 μ M, respectively; [Figure S1C](#)). Next, we applied Seurat ([Butler et al., 2018](#)). Seurat is a dimensionality reduction approach that quantifies variation (or “dispersion”) with a score of signal variability after comparing multiple data dimensions (12, in our case, considering the integration of 4 conditions and 3 RNA processing states; [Figures 1D](#), graph). The twelve expression values for each of the $n = 867$ most-dispersed coding genes (out of $n = 6,136$ catalogued, as expressed in at least one condition) were converted into an expression “admixture” representing only two dimensions using the t-distributed stochastic neighbor embedding (t-SNE) algorithm after the application of the clustering method shared nearest neighbor (SNN) modularity optimization, which segregated the expression admixture values into $n = 17$ modules (M) that represent seventeen gene subsets with distinct transcriptomic features ([Figures 1D](#) and [S1D](#); [Table S1](#)). We note that differences between RNA processing steps, treatments, cells, or a combination of them can generate dispersion.

The distinct distribution of genes throughout the t-SNE plot supports the successful segregation of the transcriptomic data. For instance, genes that would be primarily regulated transcriptionally, such as M1–2, are distinctively located toward the top-left side of the t-SNE plot ([Figures 1E](#), [1F](#), [S1E](#), and [S1F](#)). On the other hand, genes that would be primarily regulated posttranscriptionally, such as M15–17, are distinctively located toward the bottom-right side of the t-SNE plot ([Figures 1E](#), [1F](#), [S1E](#), and [S1F](#)). Well-characterized p53-regulated genes accumulate in a single module, M11, supporting that at least some modules genuinely represent underlying regulatory principles (e.g., p53 targets *CDKN1A*, *MDM2*, *GDF15*, *TP53I3*, *DIT4*, *IER3*, *IER5*, *EGR1*, and *BTG2*).

Next, we sought to identify the gene modules that concentrate the highest signal dispersion between A2780 and repeatedly treated A2780cis cells. Approximately 50% of the most differentially expressed genes accumulate with significance in only five modules, M10–14 (χ^2 -test, $p < 0.05$); the rest of the genes distribute sparsely throughout the other modules ([Figures 1G](#) and [S1G](#)). Importantly, M10–14 modules are almost entirely constituted by the subset of the most differentially expressed genes, which suggests that the underlying regulatory principles within each module are associated with repeated drug treatment. In contrast, the other 50% of the most differentially expressed genes belong to modules in which many other transcripts are not part of this subset, thus suggesting a weaker association of the underlying regulatory principles with the drug treatment. We were, therefore, particularly interested in the underlying mechanisms driving the expression of M10–14 genes. M10–14 genes are enriched in several Gene Ontology (GO) terms associated with development, which we found relevant considering that dedifferentiation is a hallmark of cancer progression and resistance ([Figures 1H](#) and [S1H](#)).

Transcription Specificity, Not Global Activity, Disturbed by Cisplatin Treatment

M10, 12, and 13 represent subsets of upregulated genes in A2780 cells, M14 represents a subset of upregulated genes in

A2780cis cells, and M11 represents a subset of upregulated genes in either A2780 or A2780cis cells but with the particularity of showing relatively robust signal in all conditions and RNA processing steps ([Figure S1D](#)). In the five modules, we observe consistent A2780- or A2780cis-associated effects across the three RNA processing steps (see, for instance, that the blue dots dominate the M13 module and that the red dots dominate the M14 module in every RNA processing step, in [Figures 1G](#) and [S1G](#)). This observation suggests that the first step, transcription, is the major contributor to differential expression in these five modules, which we found intriguing in the context of prior work. Prior studies based on reconstituted cell systems, cisplatin-modified probes, and the use of high cisplatin doses ([Ang et al., 2010](#)), such as 100 μ M ([Becker et al., 2014](#)), 80–700 μ M ([Rosenberg and Sato, 1993](#)), 100–200 μ M ([Heminger et al., 1997](#)), or 500 μ M ([Melnikov et al., 2016](#)), suggested that the drug induces global transcriptional shutdown by either blocking RNA polymerase II (RNAPII) progression during transcription elongation ([Becker et al., 2014](#); [Harder and Rosenberg, 1970](#); [Heminger et al., 1997](#); [Melnikov et al., 2016](#); [Rosenberg and Sato, 1993](#); [Sato et al., 1996](#)) or as a byproduct of drug-stimulated cell death ([Marissen and Lloyd, 1998](#)). However, GRO-seq analysis shows that both cell populations, A2780 and A2780cis, exhibit no apparent signs of global transcription elongation blockage after three continuous days of cisplatin treatment with an IC₅₀ dose ([Figures S2A](#) and [S2B](#)). We note that, at the same time, the cells show robust signs of having initiated apoptosis (as it will be shown later in [Figure 6C](#)). We do observe major dysregulation of transcription initiation in an A2780- or A2780cis-specific manner ([Figures S2A](#), [S2C](#), and [S2D](#)).

Integrating Chromatin Features to the Modular Segregation of the A2780 Transcriptome

Transcription initiation is regulated by promoters and enhancers. On these regions, cisplatin is known to induce selective accumulation of machinery of nucleotide excision repair (NER), which removes cisplatin-DNA adducts, protecting them from lasting mutational toxicity ([Hu et al., 2016](#)). On the other hand, the effects of cisplatin on chromatin at these regions and the potential consequences on transcription initiation remain unclear. Thereby, we profiled three typical features of promoters and enhancers (H3K4me3, H3K4me2, and H3K27ac) by chromatin immunoprecipitation sequencing (ChIP-seq) in the same experimental conditions as in the transcriptomic tests ([Figure 1A](#)). These analyses identified $n = 55,113$ regions with at least one histone mark in at least one treatment condition in A2780 or A2780cis cells, or both. On a global scale, H3K4me3 profiles are largely similar, whereas H3K4me2 profiles and, especially H3K27ac profiles, are relatively dissimilar between A2780 and A2780cis cells regardless of the drug treatment ([Figure 2A](#)). We performed unsupervised K-means clustering analysis integrating the twelve chromatin measurements and based on 6-kb-wide windows centered at each location ([Figure 2B](#)). We set to run this test with $k = 28$ clusters but obtained similar results with

(E) Principal-component analysis (PCA) of average distances among regions of different chromatin patterns. Circles are proportional to the number of regions.
(F) Pairwise correlation matrix of close chromatin pattern proximities (10- and 25-kb windows; see [Figure S2H](#) for 50-kb windows). Patterns are indicated. See also [Figure S2](#).

$k = 20, 24$, and 35 clusters, as expected based on an analysis of mean adjusted figures of merit (FOM) values (Figure S2E). Fourteen clusters (or “fixed” patterns, F1–14) do not show major organizational alterations ($n = 16,231$, 30%; Figure 2B). The other fourteen clusters (or “variable” patterns) contain organizational differences either between treatments, populations, or both ($n = 38,882$, 70%). Notably, all variable patterns except one (“parental and resistant-specific” [P/R1]) show robust A2780-only or A2780cis-only features (referred to as “parental-specific” P2–5 and “resistant-specific” R2–10, respectively; Figure 2B). Also relevant, variable patterns rarely colocalize with transcriptional start sites (TSS) (9%, compared to 70% in fixed patterns; see colored bars on the side of each panel in Figure 2B). The majority of variable regions are responsive to the 3-day treatment ($n = 27,680$, 71%; e.g., compare “–” and “C” for R2 in Figure 2B). In combination, these analyses reveal a high number of differences in chromatin organization between A2780 and A2780cis cells that affect primarily enhancers and that are primarily sensitive to the 3-day drug treatment, which suggests that some of these regions contribute to the differential drug sensitivity between A2780 and A2780cis cells.

We leveraged the modular segregation of the coding transcriptome and the clustering of genomic regions to integrate these two classes of datasets. For this analysis, we set a 200-kb window based on the prior observation that most enhancer:promoter interactions occur within this distance (Chepelev et al., 2012; Dekker et al., 2013; Fulco et al., 2019; Mumbach et al., 2017; Ron et al., 2017). By modules, only M12–14 are frequently and infrequently at the same time within 200 kb to one or more variable patterns over random expectation (which we refer to as enrichment and exclusion, respectively; χ^2 test, $p < 0.001$; Figures 2C and S2F). For instance, M13 genes are frequently within 200 kb from P2–4 patterns (A2780-specific genes and features, respectively), whereas these genes are infrequently within this distance from R2–6/8–10 or P/R1 patterns (Figures 2D, S2F, and S2G). In contrast, M14 genes are frequently within 200 kb from R5/6 patterns (A2780cis-specific genes and features, respectively), whereas these regions are infrequently within 200 kb from P2/3, R3/4, or P/R1 patterns (Figures 2D, S2F, and S2G). The other modules, including M10/11, are located either frequently or infrequently within 200 kb from one or more variable pattern(s), or randomly about all of them (Figures 2C, S2F, and S2G). In particular, M15–17, the three modules with the poorest transcriptional activity (Figures 1E and S1E), avoid proximity to any variable pattern, in support that M15–17 genes are primarily regulated posttranscriptionally (Figures 2C and S2F).

Two non-mutually exclusive hypotheses could explain why genes that belong to the same module can be proximal to different patterns (e.g., M13 relative to P2–4 patterns). First, it could be that genes and chromatin patterns associate as pairs (i.e., one gene per one pattern) and that different pairs can occur within the same module. Alternatively, it could be that genes that belong to the same module are proximal to the same array of neighboring chromatin patterns (i.e., one gene for multiple patterns). On a global scale, our analyses favor the second model, although without discarding the first model for some individual cases. Briefly, we performed principal-component analysis (PCA), revealing that some variable patterns show similarity in

their repertoires of proximities to the other 27 chromatin patterns, which suggests that each of these patterns is similarly positioned in the genome relative to the rest (Figure 2E). Furthermore, a pairwise comparison of frequencies at which the regions of each chromatin pattern can be found within a range (10, 25, or 50 kb) of the regions of another chromatin pattern reveals some frequent selective proximities (e.g., P2/3/5 or R2–6/9; Figures 2F and S2H).

Candidate Drivers of Chromatin Alterations in Chronically Cisplatin-Treated Cells

To identify drivers of the chromatin and transcriptional differences between A2780 and A2780cis cells, we applied the Hypergeometric Optimization of Motif EnRichment (HOMER) tool, which is a *de novo* motif-discovery algorithm well suited to search DNA-binding motifs in large-scale chromatin datasets (Heinz et al., 2010). We found robust enrichment of the CTCF motif in R8 and R9 ($p = 1e-410$ and $p = 1e-236$; Figure S3A) and the p53 motif in P/R1 and R3 ($p = 1e-121$ and $p = 1e-87$; Figure S3A), which we corroborated using ChIP and p53 ChIP-seq analysis (Figures 3A, S3B, and S3C). None of these four patterns, however, is particularly proximal to any of the five modules accumulating the most dysregulated genes between A2780 and A2780cis cells (Figure S2F). As an alternative motif-searching tool, therefore, we applied Taiji (Yu et al., 2017). Taiji is a sophisticated approach based on the PageRank algorithm that integrates motif analysis and expression and ranks motifs by importance in a predicted regulatory network. In particular, we used GRO-seq and nonclustered H3K27ac/H3K4me2 ChIP-seq data to increase the statistical power of this analysis. In addition, we focused on motifs whose transcription factors are encoded by the subset of differentially expressed genes, as we considered that it might strengthen their candidacy as functionally relevant regulators. Thru this analysis, we found abundance of developmental transcription factors—relevant considering the overall enrichment of developmental GO terms in M10–14 (Figure 1H). The highest ranks corresponded to Islet-1 (ISL1), PAX2, PRRX1, ZIC1, and ATF5 in A2780 cells and GATA2, NKX2.5, SNAI2, MZF1, and EGR1 in A2780cis cells (Figure 3B in red and blue, respectively; see ISL1 and EGR1 scores in Figure 3C).

To interrogate the potential role of developmental regulators in driving transcriptional dysregulation between A2780 and A2780cis cells, we found particularly attractive the case of ISL1, which is a member of the LIM-homeobox family. ISL1 is a master developmental regulator involved in cell survival and apoptosis, as well as in mesenchymal transitions (Ching et al., 2018; Li et al., 2014, 2017; Lu et al., 2014; Xiang et al., 2018). ISL1 is one of the most highly expressed transcription factors in A2780 cells, although its expression is low in A2780cis cells (see below). In the Depmap database, we observe *ISL1* expression in 36 of the 48 lines of the ovarian cancer collection (75%) and in many non-ovarian cancer lines (Figures S3D and S3E). In The Cancer Genome Atlas (TCGA) database, we observe *ISL1* expression in two-thirds of serous ovarian carcinomas (Figure S3F). In the Genotype-Tissue Expression (GTEx) database, we observe that ISL1 is not highly expressed in healthy ovary tissue, but it is relatively enriched in proximal gynecologic tissues (Figure S3G). In summary, the expression of the *ISL1* gene is

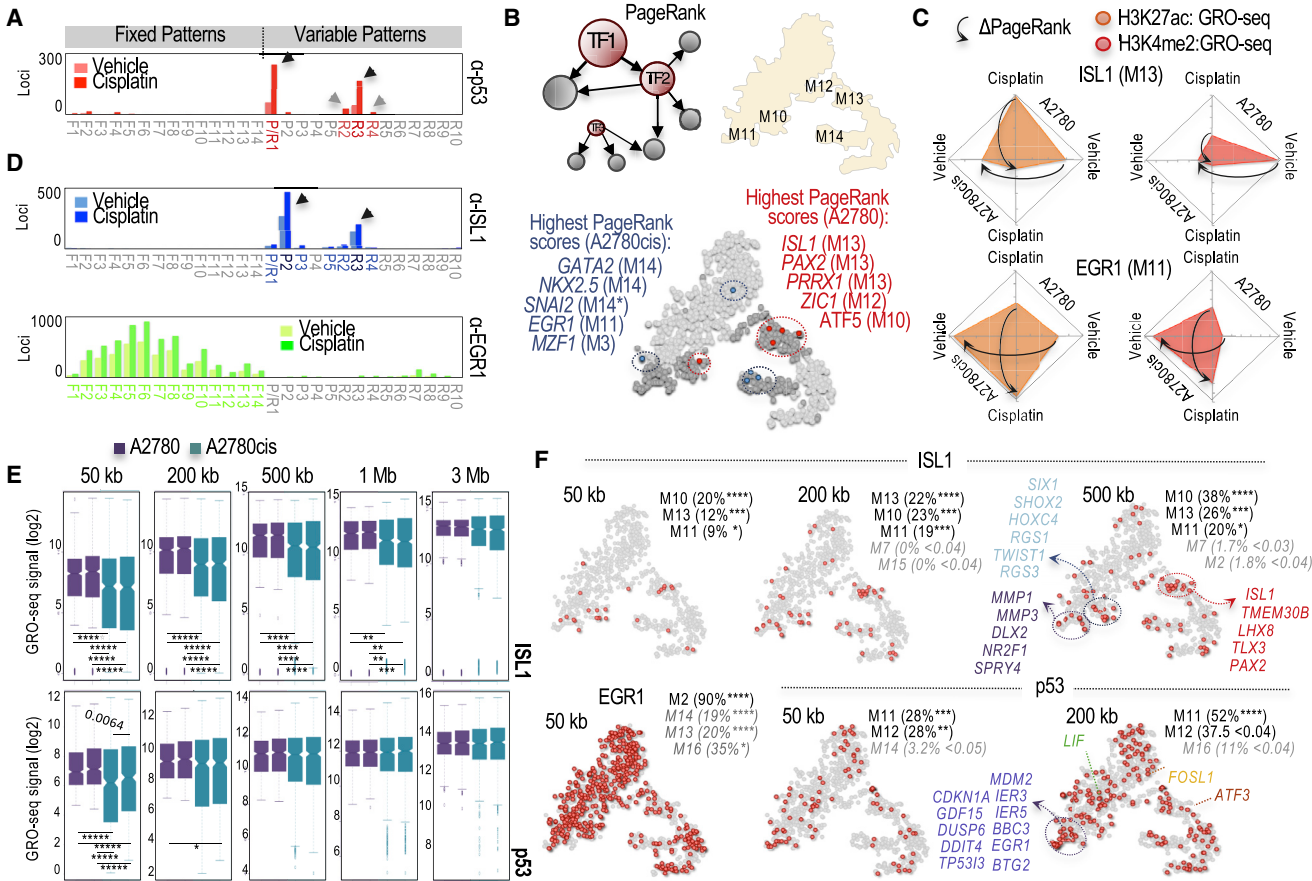


Figure 3. ISL1 Is a Potential Major Regulator of Differential Expression between A2780 and A2780cis Cells

(A and D) Distribution of p53 in (A) and ISL1 and EGR1 in (D) ChIP-seq peaks in A2780 cells by chromatin patterns.

(B) Illustrative scheme of a PageRank-based network. Lists of transcription factors and motifs with the highest PageRank scores in A2780 (in red) or A2780cis (in blue) cells. Analysis based on H3K27ac:GRO-seq and H3K4me2:GRO-seq data. *, motif assigned to M4 in the clustering analysis but colocalizing with M14 (see Figure 1D).

(C) Radar plots depicting PageRank scores for ISL1 and EGR1. Arrows indicate (Δ) differences in PageRank scores.

(E) Boxplots of GRO-seq signal enrichment (\log_2 scale) by cell and condition within different distances (50 kb to 3 Mb, as indicated) from ISL1 (top) or p53 (bottom) ChIP-seq peaks in A2780 cells. Conditions (in this order): A2780-vehicle, A2780-cisplatin, A2780cis-vehicle, and A2780cis-cisplatin. Welch two-sample t-test; * $p \leq 0.005$, ** $p \leq 10^{-3}$, *** $p \leq 10^{-4}$, **** $p \leq 10^{-5}$, ***** $p \leq 10^{-6}$.

(F) Dispersed genes within different distances from ISL1, EGR1, or p53 ChIP-seq peaks. The names of representative genes are included. Modules with higher (in black) or lower (in gray italics) gene enrichment than randomly expected are indicated, as well as the percentage of the genes over the total in each module. χ^2 test; * $p \leq 10^{-3}$, ** $p \leq 10^{-4}$, *** $p \leq 10^{-5}$, **** $p \leq 10^{-6}$.

See also Figure S3.

not a rarity of ovarian cancer A2780 cells, although it is rather highly expressed in these cells.

ISL1 ChIP-seq analysis in A2780 cells reveals dense areas of ISL1 occupation, characterized by 10–20 “neighboring” binding events distributed across genomic stretches of thousands of kilobases (examples will be shown in Figures 4B, S4A, and S4C). In contrast, p53 binding tends to be isolated (see examples in Figure S3B). ISL1 binding is highly selective of A2780-specific P2 and A2780cis-specific R3 regions (Figure 3D, ISL1), two patterns that are proximal between them more often than randomly expected (Figures 2F and S2H). Integration of ISL1 ChIP-seq and GRO-seq data shows transcriptional differences around ISL1 peaks between A2780 and A2780cis cells, which can span over a distance of 1 Mb (Welch two-sample t test, $p < 0.001$; Fig-

ure 3E). Due to this long distance, we suspect that ISL1 may influence additional chromatin patterns based on their proximity to P2 and R3, such as P3/5 and R2/4 (Figures 2F and S2H). ISL1 peaks tend to locate within the range of 50 to 500 kb from M10/11/13 genes, three of the five most dysregulated modules (χ^2 -test, $p < 0.001$; Figure 3F, ISL1). In contrast, EGR1 (whose motif is distinctively enriched in A2780cis cells; Figure 3B) does not locate proximal to any of the five most dysregulated modules, as determined by ChIP-seq (χ^2 test; Figures 3D and 3F, EGR1); p53 peaks, on the other hand, are proximal to M11/12 (χ^2 -test; Figure 3F, p53). In combination, these analyses suggest that ISL1 is a candidate regulator of broad and diverse differential expression and chromatin organization between A2780 and A2780cis cells.

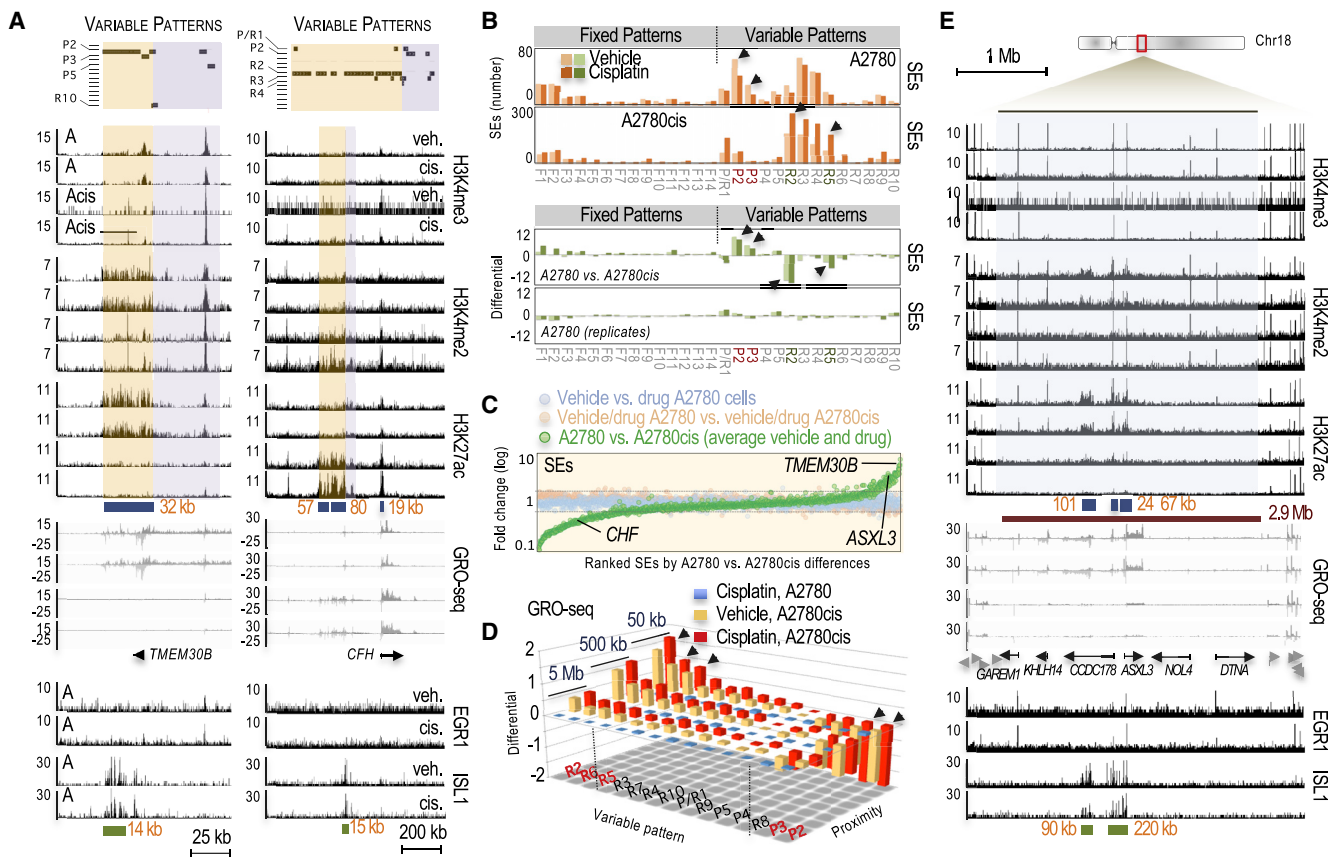


Figure 4. SEs Are Associated with Major Organizational and Expression Differences between A2780 and A2780cis Cells

(A and E) From top to bottom, read-density tracks of the indicated ChIP-seq and GRO-seq signal in A2780 (A) and A2780cis (Acis) cells after 3-day vehicle (veh.) or cisplatin (cis.) treatment. The y axis indicates sequencing read density. Green bars indicate dense areas of ISL1 peaks, blue bars indicate candidate SEs, and the red bar highlights a 2.9-Mb-wide region with low signal in A2780cis cells. Above in (A), shown are 6-kb bins of variable patterns in the same order as depicted in Figure 2B, corresponding to the peach- and purple-colored regions.

(B) The top two panels show distribution of SEs by clusters and treatment in A2780/A2780cis cells. The bottom two panels show differential of the relative fraction of SEs over the total by chromatin pattern between A2780 and A2780cis cells and between biological replicates, as indicated.

(C) Differential in H3K27ac accumulation (fold change, log₁₀) at the set of ROSE-defined SEs in the following comparisons (SEs ranked by H3K27ac signal in vehicle A2780 cells): 3-day vehicle- versus cisplatin-treated A2780 cells (in blue), cisplatin responsiveness in A2780 versus A2780cis cells (in orange), and combined 3-day vehicle/cisplatin-treated signal in A2780 versus A2780cis cells (in green).

(D) Differential GRO-seq signal around each of the 14 variable patterns (distances: 50-kb, 500-kb, and 5-Mb regions) in 3-day cisplatin-treated A2780 and 3-day vehicle- and cisplatin-treated A2780cis cells relative to 3-day vehicle-treated A2780 cells. Arrows highlight the five cases with the strongest effects.

See also Figure S4.

ISL1 Super-Enhancers Are among the Most Dysregulated Regions in A2780cis Cells

Notably, ISL1 binding overlaps clusters of enhancers conventionally referred to as super-enhancers (SEs) (see examples in Figures 4A, 4E, and S4A–SC). SEs are long *cis*-regulatory elements characterized by robust H3K27ac accumulation (Hnisz et al., 2013; Lovén et al., 2013; Whyte et al., 2013). However, H3K27ac is not uniformly distributed across these elements, which may explain the model of one gene for multiple patterns mentioned above (see, for example, the annotation shown above Figure 4A in which ISL1-occupied P2 and R3 regions represent two different segments of the same SE-like region). We next applied the Ranking Ordering of Super-Enhancer (ROSE) algorithm to catalog the SE program in A2780 and A2780cis cells (Hnisz et al., 2013; Lovén et al., 2013; Whyte et al., 2013).

ROSE identified 100–415 SEs, depending on the treatment, that primarily overlap with variable regions (Figure 4B, top two panels). Although mostly similar between A2780 and A2780cis cells, the SE programs selectively differ in the number of P2/3 and R2/5 regions (Figure 4B, differential panels). Furthermore, to corroborate that these selective differences correspond to robust alterations in H3K27ac accumulation, we compared the levels of this histone mark in our four cell culture conditions at SE regions, revealing major differences in a large subset not observed when comparing replicates or vehicle and cisplatin treatments in A2780 and A2780cis cells (Figure 4C). Importantly, P2/3 and R2/5 (in addition to R6) regions accumulate the strongest and wider differential transcription between A2780 and A2780cis cells (Figure 4D; see differences spreading over kilobases in Figures 4E, S4A, and S4C). Together, these results reveal that the differences in the SE

program between A2780 and A2780cis cells are associated with some of the most robust events of differential chromatin organization and transcription between these cells.

Before interrogating potential mechanisms driving the selective SE redistribution, we sought to confirm this feature in a second cancer model. In particular, we leveraged H3K27ac ChIP-seq data generated by the ENCODE Consortium to annotate SEs in the lung cancer A549 line (Figure S5A). We also leveraged expression data generated in parental and chronically cisplatin-treated A549 cells (Fang et al., 2017). We identified $n = 1,238$ differentially expressed genes (adjusted $p = 0.01$, fold change [FC] = 2), and $n = 105$ are located within a distance of 50 kb from the center of a SE (out of the $n = 693$ genes located within this distance to a SE) in chronically cisplatin-treated A549 cells or A549cis cells (Figure S5B). In this second model, therefore, we also observe a large subset of SE-associated genes dysregulated after repeated drug treatment. Furthermore, we confirmed that an IC_{50} dose of cisplatin for 3 days does not block transcriptional elongation on a global scale (Figure S5C).

ISL1 Is a Major Contributor to Long-Term Cisplatin-Induced Differential Expression

ISL1 expression is substantially lower in A2780cis than in A2780 cells, which is corroborated at the protein level (Figures 5A and 5B). To interrogate whether ISL1 is a driver of broad expression dysregulation after repeated cisplatin treatment, we next applied the lentiviral CRISPR/dCas9-KRAB inhibition (CRISPRi) system in A2780 cells and the CRISPR/dCas9-VP64 activation (CRISPRa) system in A2780cis cells. In both systems, we used two different pairs of guide RNAs (gRNAs) as replicates (#1 and #2). The CRISPRi system induces ISL1/ISL1 downregulation, and the CRISPRa system induces ISL1/ISL1 upregulation, as expected (Figures 5C, 5D, and S5D). RNA-seq analysis reveals that 32%–33% and 74%–76% of the $n = 867$ dispersed genes in CRISPRi-modified and CRISPRa-modified cells, respectively, show altered expression compared to unmodified cells (differences established with $p < 0.001$). Moreover, the top 100 most differentially expressed genes accumulate with significance in the five modules, with the most dysregulated genes between A2780 and A2780 cells, in addition to M2/3/8 (χ^2 test, $p < 0.001$; Figures 5E and 5F). Also, in many cases, the direction of the effects is the expected and antagonistic between CRISPRi and CRISPRa cells (e.g., ASXL3 in Figures 5G and 5H; PRRX1, SNAI2, and NKX2-5 in Figures S5E and S5F). In other instances, however, we observe the expected effect only in the CRISPRi system (e.g., TMEM30B and LINC02106; Figures 5C, 5D, 5G, and 5H) or in the CRISPRa system (e.g., SIX1, PTBP2, and CHF; Figures 5G and 5H). It appears, therefore, that the effects of the CRISPR-modified systems are only partially expected, which could also be explained by the partial effects on the *ISL1* gene (compare scales in the RNA-seq tracks shown in Figures 5C and 5D). On a global scale, the largest subsets of dysregulated genes in the CRISPRi/a systems belong to the M10/11/13 modules (Figures S5G and S5H), which is expected, because M10/11/13 genes are proximal to ISL1 peaks (Figure 3F, ISL1).

To also examine the SE program in the CRISPRi/a systems, we profiled H3K27ac and applied the ROSE algorithm. Although the number of SEs segregated by chromatin patterns is almost iden-

tical between replicates, it is different between CRISPRi-modified and unmodified A2780 cells with selectivity of chromatin patterns (Figures 5I and 5J, top and bottom panels, respectively). The largest losses occur in R3/4 SEs, which are occupied by ISL1 in A2780 cells, especially the former (Figure 5I, bottom panel; Figure 3D, ISL1). Thus, ISL1 might play a direct inhibitory role in the formation of some R3/4 SEs in A2780 cells. The fact that we did not observe obvious effects in P2 regions—the most robustly occupied regions by ISL1 in A2780 cells—suggests some resilience to lose these SE regions; potentially, the reason is that P2 regions are the most robustly occupied by ISL1 (Figure 5I, bottom panel; Figure 3D, ISL1). By comparing the SE profiles between CRISPRa-modified and -unmodified A2780cis cells, we observe effects on R3 regions again, but, unexpectedly, instead of an increase in the number of SEs, we observe a loss as we do in CRISPRi-modified A2780 cells (Figure 5J, bottom panel). Without understanding this effect yet, we could confirm the expected increases in H3K27ac accumulation matching with expression upregulation in relevant loci (e.g., in ASXL3, SIX1, CHF, and LINC02106; Figure 5K, compare to Figures 5G and 5H). In combination, these results suggest that ISL1 is a major regulator of differential expression and SE organization between A2780 and A2780cis cells. Paradoxically, reintroducing ISL1 in low-ISL1-expressing A2780cis cells does not induce, in many cases, the expected rescue of ISL1-associated features but instead induces their further loss, thus suggesting a change in how ISL1 contributes to the biology of A2780 cells after repeated cisplatin treatment. We further address this conundrum in a later section.

Effects of Cisplatin on ISL1 Protein and Gene Expression

Cancer therapy is often regarded as a Darwinian process of clonal selection. We, therefore, interrogated whether low-ISL1-expressing A2780cis-like cells may (pre)exist in the A2780 population by using the anti-ISL1 antibody (Figure S6A). We measured ISL1 protein levels at a single-cell scale by using indirect fluorescence-activated cell sorting (FACS). FACS analysis of $n = 100,000$ fixed A2780 and A2780cis cells reveals a spectrum of ISL1 expression values but with the levels in each predominant subpopulation being higher in A2780 than A2780cis cells, which is replicated by the CRISPRi/a systems (Figures 6A, 6B, and S6B). Still, we could observe a small A2780 subpopulation that shows ISL1 levels analogous to those observed in the predominant A2780cis subpopulation (i.e., low). We determined that this subpopulation represents 8%–9% of the A2780 population in an analysis of $n = 1$ million A2780 cells or approximately a 1:11 to 1:13 ratio (Figure S6C). Initially, therefore, these observations could be supportive of a model of preexistence followed by clonal selection associated with ISL1 expression and induced by the treatment. We note, however, that 3-day drug exposure does not enrich for the low-ISL1-expressing A2780 subpopulation, suggesting that ISL1 levels do not represent an advantage for selection (Figure 6C, top). Furthermore, we isolated $n = 1.7$ million low-ISL1-expressing and $n = 1.7$ million high-ISL1-expressing A2780 cells and performed RNA-seq analysis after reversing fixation (Figure 6D, FACS and RNA-seq track). Unsupervised clustering analysis reveals that low- and high-ISL1-expressing A2780 cells are indistinguishable on a transcriptome-wide scale

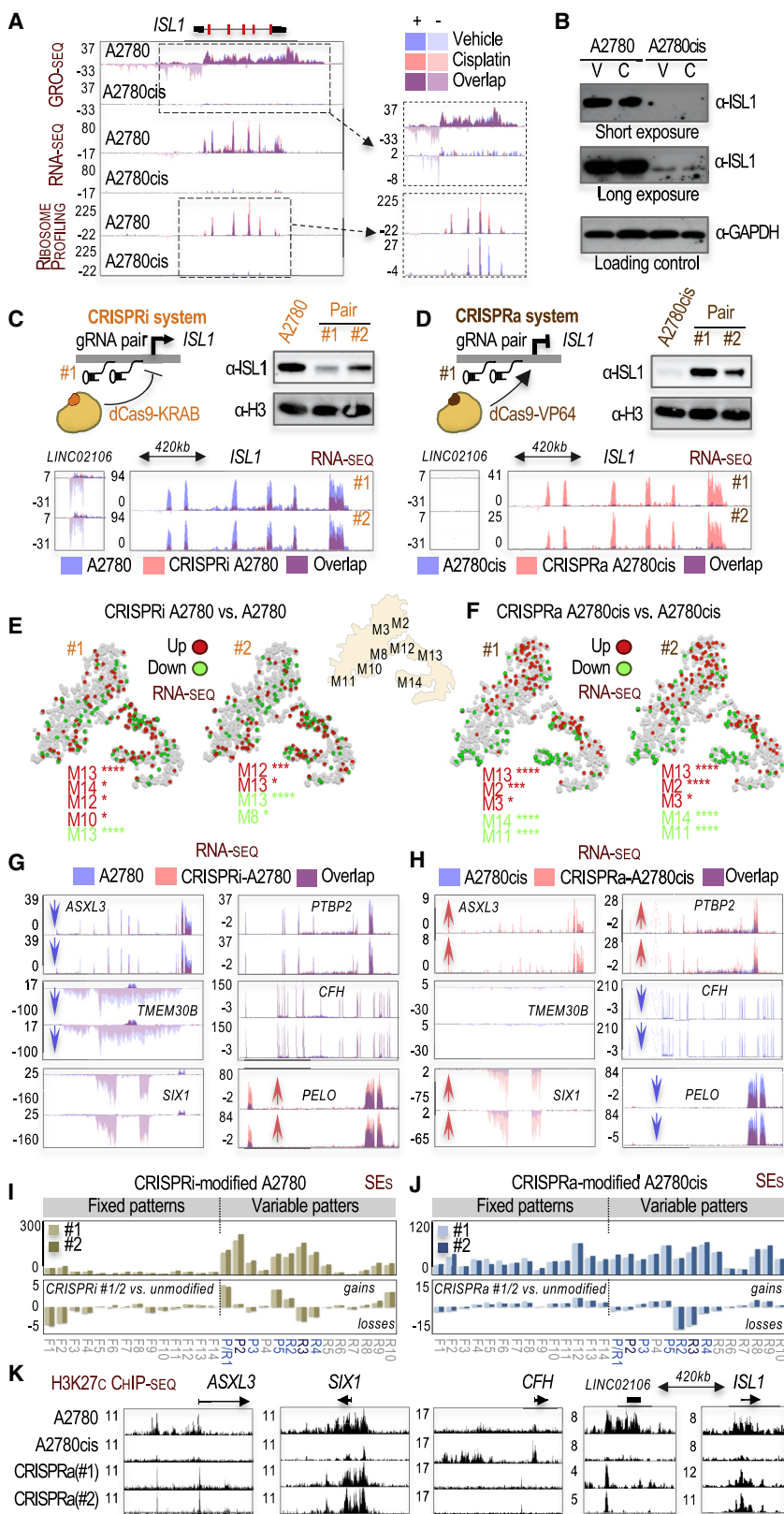


Figure 5. ISL1 Is a Master Regulator of the A2780 Transcriptome

(A) GRO-seq, RNA-seq, and ribosome profiling signal across the *ISL1* locus in A2780 and A2780cis cells. Reads from vehicle and cisplatin treatments and positive and negative strands were differently colored, as indicated. 5' and 3' UTRs are shown as black bars, exonic regions are shown as red bars, and intronic regions are shown as a black line. Identical scales were used in each assay. Zoomed images and adjusted scales are shown to the right. (B) Western blot analysis of ISL1 and GAPDH expression in 3-day vehicle- and cisplatin-treated A2780 and A2780cis cells.

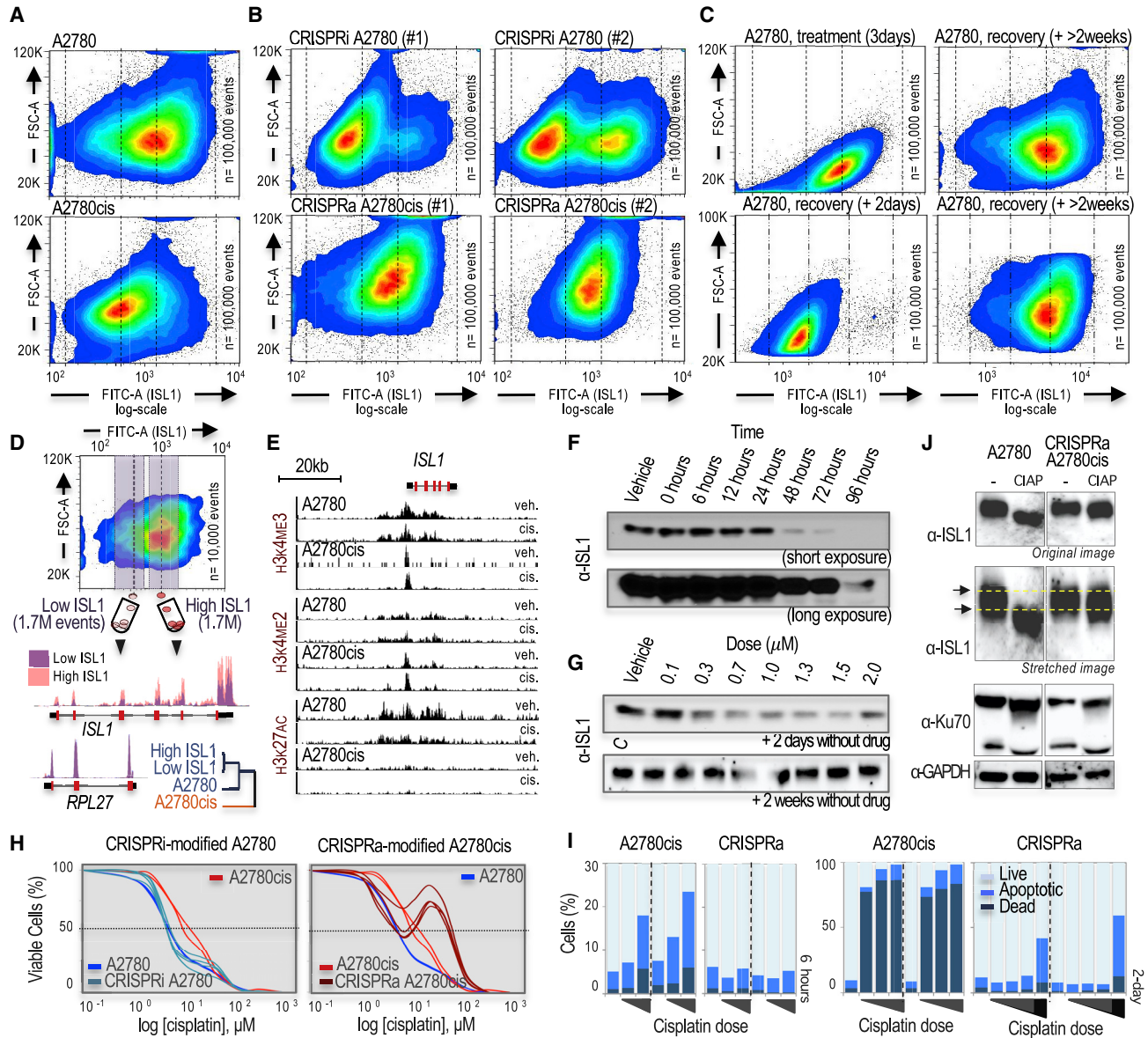
(C and D) Lentiviral-based CRISPR-dCas9-KRAB/VP64-mediated editing of the *ISL1* promoter in A2780 (C) and A2780cis (D) cells by using the CRISPRi and CRISPRa systems, respectively, and using two different pairs of gRNAs (#1 and #2). (Top) *ISL1* levels examined by western blotting. (Bottom) *ISL1* levels examined by RNA-seq, including signal at the SE region located 420 kb upstream *ISL1* gene overlapping *LINC02106* (see Figure S4C as reference).

(E and F) Top 100 most upregulated (in red) and top 100 most downregulated (in green) dispersed genes in the CRISPRi/a-modified cultures. Modules with an enriched number of cases are indicated (χ^2 test: * $p \leq 10^{-3}$, ** $p \leq 10^{-4}$, *** $p \leq 10^{-5}$, **** $p \leq 10^{-6}$).

(G and H) RNA-seq tracks of dispersed genes in CRISPRi/a-modified and unmodified cells. Reads from positive and negative strands are differently colored. Scale indicated. CRISPRi/e-modified replicates (top and bottom tracks) are compared to the same unmodified control. Arrows indicate the effects of the CRISPR modification. Genes indicated.

(I and J) Normalized distribution of SEs by clusters in the two pairs of CRISPRi/a-modified sublines (top panel), and differential of the relative fraction of SEs over the total by chromatin pattern between modified lines and parent A2780 (I) or A2780cis cells (J) (bottom panel).

(K) H3K27ac ChIP-seq signal in CRISPRa-modified and parent A2780 and A2780cis cells as indicated. See also Figure S5.

**Figure 6. ISL1 Dysregulation after Chronic Cisplatin Treatment**

(A–C) Singlet distribution of forward scatter A (FSC-A; x axis) versus FITC-A signal (Alexa Fluor-488; y axis) identified by FACS analysis in fixed A2780 and A2780cis (A), in CRISPRi/a-modified cells (B), and in A2780 cells treated for 3 days with cisplatin IC₅₀ (C) and adding no additional time, 2 days, or 2 weeks (in duplicate) of recovery without drug. As reference, dashed lines indicate the position of the predominant subpopulation and maximum and minimum margins for panels in (A). Each analysis corresponds to n = 100,000 sorting events.

(D) FACS sorting of n = 1.7 million fixed low-ISL1-expressing and n = 1.7 million fixed high-ISL1-expressing cells, decrosslinking, and RNA-seq analysis. Panel shows FACS analysis of the first n = 10,000 sorting events. Tracks show RNA-seq signal along the *ISL1* and *RPL27* (as reference) loci. Other genomic regions shown in Figure S6D. Hierarchical clustering of high-ISL1- and low-ISL1-expressing A2780 cells, bulk A2780 cells, and A2780cis cells.

(E) H3K4me3, H3K4me2, and H3K27ac ChIP-seq signal along the *ISL1* locus in A2780 and A2780cis cells after 3-day of vehicle (veh.) or cisplatin (cis.) treatment.

(F) Time-course analysis of ISL1 protein abundance at the indicated time point after the end of a 2-day cisplatin treatment (2.0 μ M) examined by western blot in A2780 cells (two different exposures).

(G) Dose-titration analysis of ISL1 protein abundance at the end of a 2-day cisplatin treatment followed by 2 days or 2 weeks of recovery without drug in A2780 cells. C, nonrecovery control.

(H) Dose-response curve of cisplatin in A2780/A2780cis and CRISPRi/a-modified cells (2-day treatment). Lines represent median values. Biological duplicates (n = 2) with six technical replicates each (n = 6). As reference, A2780 and A2780cis data are identically shown in both panels.

(legend continued on next page)

and are different from the A2780cis population (**Figure 6D**, clustering). In combination, these analyses suggest that although A2780cis-like cells preexist in the A2780 population with regard to low levels of *ISL1* expression, this feature represents a transcriptomic singularity accompanied by only a few other transcriptomic characteristics in A2780cis cells, such as low *TMEM30B* and *LINC02106* expression (**Figure S6D**). In summary, we propose that A2780cis cells would evolve during the treatment rather than preexist prior to cisplatin treatment.

In our goal to interrogate how *ISL1* expression could decrease after repeated cisplatin treatment, we noticed that 3 days of exposure induces an approximately 50% reduction in H3K27ac accumulation at and around the *ISL1* gene (**Figure 6E**). This effect is not matched by *ISL1* transcriptional downregulation (**Figures 5A** and **5B**), although *ISL1* protein levels abruptly decay 2 days into recovery after this treatment, when apoptosis is already underway. Specifically, apoptosis typically includes an early step of cell-size shrinkage that results from intracellular imbalances of monovalent ions (Bortner and Cidlowski, 2003). This feature is obvious after the 2-day recovery (**Figure 6C**, top left; **Figures S1B** and **S6E**). We also corroborated *ISL1* decay by western blot (**Figure 6F**), finding that it is dose dependent and transient, as it is not observed after 2 week of recovery (**Figures 6C** and **6G**). Together, we suspect that *ISL1* decay accompanies the early steps of apoptosis and might be stabilized if cells repeatedly undergo these steps without reaching the late stages of the apoptotic process, as suggested by the observation that *ISL1* levels are stably low in repeatedly treated A2780cis cells; yet, this feature does not seem to provide an advantage for drug-mediated selection. Interestingly, there is a SE-like region located 420 kb upstream the *ISL1* gene occupied by *ISL1* (**Figure S4C**). This region generates noncoding transcripts that are downregulated after *ISL1* downregulation in the CRISPRi system (**Figure 5C**), thus suggesting that the *ISL1* locus might be regulated by a positive feedback loop.

Linking *ISL1* to the Acquisition of Transcriptomic Features after Repeated Cisplatin Treatment

As mentioned above, we do not have evidence for cisplatin favoring the selection of low-*ISL1*-expressing cells (**Figures 6A** and **6C**). In the same line, CRISPRi-modified A2780 cells show similar drug sensitivity as unmodified A2780 cells (**Figure 6H**, left panel, dark and light blue lines). Surprisingly, however, CRISPRa-modified A2780cis cells show a more than 3-fold increase in IC_{50} values relative to unmodified A2780cis cells (**Figure 6H**, right panel, dark and light red lines). The dose-response curve in these super-resistant cells deviates from the typical sigmoidal shape, appearing triphasic with two points of inflection (**Figures S6F** and **S6G**). Flow cytometry analysis corroborates the super-resistance of CRISPRa-modified A2780cis cells (**Figure 6I**).

In an initial effort to understand the differential effects resulting from the modulation of *ISL1* levels in A2780 and A2780cis cells,

we focused on a slight difference in the electrophoretic mobility of the *ISL1* band when comparing A2780 and A2780cis cell extracts (**Figure 5B**, long-exposure panel). In the context of other cells, a similar shift has been attributed to phosphorylation because it is reversible by alkaline phosphatase treatment (Ando et al., 2003). We treated A2780 cellular extracts with alkaline phosphatase (CIAP), and this treatment shifts the *ISL1* electrophoretic mobility in A2780 cell extracts to look A2780cis-like (**Figure 6J**, left panels). In contrast, the *ISL1* electrophoretic mobility in cell extracts of CRISPRa-modified A2780cis cells is similar to the electrophoretic mobility of the protein observed in A2780 cells but is insensitive to CIAP treatment (**Figure 6J**, right panels). Counterintuitively, therefore, these results suggest that although the *ISL1* level is rather low in A2780cis cells, it can play a role in cell survival as, potentially, an acquired feature induced by the treatment.

DISCUSSION

Cancer cells are complex adaptive systems that can be remarkably resilient to drug-induced cell death (Salgia and Kulkarni, 2018). In some cases, this resilience is acquired or enhanced during drug treatment through a process of adoption of chromatin and transcriptomic features absent before treatment (Bradner et al., 2017; Easwaran et al., 2014; Flavahan et al., 2017; Knoechel et al., 2014; Koppikar et al., 2012; Liau et al., 2017; Roesch et al., 2013; Shaffer et al., 2017; Sharma et al., 2010). In melanoma cells, for instance, a nonresistant subpopulation in a “preresistant” state gradually acquires the resistant transcriptomic program through a dedifferentiation mechanism of chromatin plasticity controlled by developmental transcription factor SOX10 and induced by the drug vemurafenib (Shaffer et al., 2017). In our study, we provide evidence of a relatively similar process of adaptation mediated by developmental transcription factor *ISL1* in response to cisplatin treatment that arises when cancer cells undergo a near-to-death experience that reorganizes the SE program. Also, it will be another example of transcription factor as a potential major contributor to disease progression (Garcia-Bassets and Wang, 2012).

We were particularly surprised by the abundance of chromatin organizational differences between A2780 and A2780cis cells and by the observation that most of them accumulate on enhancers and are sensitive to the 3-day drug treatment; thus, they likely contribute to the differential drug sensitivity observed between these cells. In support of this possibility, most drug-induced effects on enhancers follow the expected “logic” when comparing the 3-day and the weeks-long drug treatments. For instance, R6 enhancers show robust H3K27ac accumulation after repeated drug exposure (in A2780cis cells compared to parental A2780 cells), and an additional round of exposure further enhances (rather than decreases) this accumulation. On the other hand, P2 enhancers show H3K27ac decay after the

(I) Percentage of live, apoptotic, and dead A2780cis and CRISPRa-modified A2780cis cells after exposure to cisplatin for 6 h or 2 days and measured by flow cytometry analysis. Identical doses used in both cell cultures, plus an additional high dose (indicated in black) administrated to CRISPRa cells after 2 days of treatment. Two biological replicates are shown in every case ($n = 2$).

(J) Effects of 1-h CIAP treatment on *ISL1* electrophoretic mobility in cellular extracts from A2780 and CRISPRa-modified A2780cis cells (western blots). See also **Figure S6**.

3-day drug treatment (in A2780 cells); apparently, the repeated drug treatment converts it into a permanent H3K27ac loss (in A2780cis cells). Only in one case, R10 regions, the effects appeared counterintuitive, as H3K4me3 accumulates in A2780 cells after repeated drug treatment (in A2780cis cells), but an additional 3-day drug treatment in A2780cis cells eliminates this histone mark from these regions. R10 regions are also unusual in that they rarely colocalize with annotated TSS despite representing H3K4me3-enriched regions. Another interesting finding is that only P/R1 enhancers show a relatively similar response to the 3-day drug treatment in A2780 and A2780cis cells, although quantitatively, the response is slightly different in each case. In the rest of regions, cisplatin-induced effects are either specific of A2780 or A2780cis cells.

We note that many of the abundant alterations identified in chromatin organization might represent noise from a functional standpoint, as previously noted for a large number of DNA-methylation alterations associated with cisplatin treatment (Li et al., 2009; Zeller et al., 2012). However, it is also possible that some chromatin alterations may silently determine cell fate, needing additional events to translate into phenotypic features. The role of chromatin in determining cell fate is well established in the context of development and differentiation (Almenar-Queralt et al., 2019; Hawkins et al., 2011; Heinz et al., 2010; Koche et al., 2011; Mikkelsen et al., 2007; Zhang et al., 2012). In this line, we have observed that the *ISL1* locus loses H3K27ac enrichment during the 3-day cisplatin treatment in A2780 cells without having an immediate effect on *ISL1* transcription. Only after repeated drug treatment, *ISL1* expression loss finally occurs.

A notorious challenge when integrating large and diverse multiomic datasets, as we performed, is the vast universe of hypotheses that could be tested. We decided to focus on the subset of the most dysregulated genes between A2780 and A2780cis cells, but we hope that other laboratories will soon benefit from our datasets to follow other leads, for example, focusing on translational dysregulation. In our case, the core finding represents the identification of a molecular mechanism driving broad transcriptional dysregulation after repeated cisplatin treatment. This mechanism is based on partial SE redistribution, which we have also observed in a second model. As it involves SE redistribution, we propose a parallel between the long-term effects induced by cisplatin treatment and a developmental-like transformation. Biologically, SEs are central to the maintenance of cancer cell identity that promotes oncogenic transcription (Sengupta and George, 2017), and they have been previously associated with drug treatment or resistance (Bao et al., 2019; Rusan et al., 2018). In our case, we have observed that SE redistribution is associated with the most robust transcriptional and chromatin dysregulated events in A2780cis cells, which is consistent by the fact that genes regulated by SEs tend to be expressed at higher levels than those controlled by typical enhancers (Lovén et al., 2013). In this regard, we suspect that our decision to focus on the subset of the most dysregulated genes led us to SEs. A second interesting chromatin rearrangement found in our study affects CTCF, which is particularly interesting based on a recent study reporting that “essential” CTCF sites for cell survival are located near genes that change expression in response to cisplatin treatment and are associated with cisplatin resistance (Fei et al., 2019).

We have identified *ISL1* as a potential mediator of cisplatin-induced SE redistribution. *ISL1* is a lineage-determinant factor that controls cell survival in different tissues (Barzelay et al., 2012; Ching et al., 2018; Huang et al., 2013; Li et al., 2014, 2017; Liang et al., 2011; Liu et al., 2014; Pan et al., 2008; Sun et al., 2008; Xiang et al., 2018). *ISL1* downregulation leads to cancer stem-cell formation (Pathania et al., 2015). *ISL1*-promoter methylation (downregulation) has also been observed in recurrent bladder cancer associated with aggressive clinicopathological characteristics (Kim et al., 2013). As *ISL1* is a cell-type-specific transcription factor, it is unlikely that a mechanism based on this particular molecule would be general. Thus, we propose that other SE regulators might be affected in other systems. Even in A2780/A2780cis cells, in fact, we chose *ISL1* as a paradigm of broad gene dysregulation but predicted a cocktail of transcription factors that may also contribute to this process (e.g., PAX2, PRRX1, ZIC1, GATA2, or NKX2.5). SE regulators are known to act cooperatively (Hnisz et al., 2013; Lovén et al., 2013; Whyte et al., 2013) and likely do so also with *ISL1*, which may explain some of the inconsistent observed effects in the CRISPRi/a systems. A role of *ISL1* in therapy resistance has been suggested in triple-negative breast cancer (TNBC) cells, in which *ISL1* overexpression inhibits cisplatin-induced cell apoptosis (Zhang et al., 2018). Other developmental transcription factors are also known to participate in cell survival in cancer cells, collectively known as “lineage survival” onco-genes, e.g., MITF (Garraway et al., 2005) and NKX2.1, SOX2, and CDX2 (Bass et al., 2009; Salari et al., 2012; Weir et al., 2007).

Finally, one of the most exciting aspects of our study is the observation of dynamism in *ISL1* expression associated with the process of apoptosis. It is essential to mention that entering apoptosis was once assumed to be an irreversible process; but recent studies suggest that some cells can recover from the brink of cell death by a process of cellular resuscitation known as anastasis (Gong et al., 2019; Gudipaty et al., 2018). The role of anastasis in response to drug treatment is still poorly understood (Tang and Tang, 2018), but we expect that our study may help to provide insights that ultimately link this process with cisplatin resistance.

In conclusion, we propose a mechanism of SE reorganization that may invoke the acquisition of an unconventional developmental identity in cisplatin-treated cancer cells. This property would be acquired after cells repeatedly undergo drug-induced near-to-death experiences. In this context, we highlight a recent study in which transdifferentiation through SE reorganization is a prerequisite for the colonization of secondary metastatic sites in colon cancer cells (Teng et al., 2019). In the future, therefore, it will be interesting to investigate whether SE reorganization associated with repeated cisplatin treatment results in an unexpected process of transdifferentiation that facilitates tumor colonization.

STAR★METHODS

Detailed methods are provided in the online version of this paper and include the following:

- KEY RESOURCES TABLE
- LEAD CONTACT AND MATERIAL AVAILABILITY
- EXPERIMENTAL MODEL AND SUBJECT DETAILS

● METHOD DETAILS

- Generation of CRISPRi- and CRISPRa-modified sub-lines
- Cell viability assays and IC₅₀ calculations
- GRO-seq, RNA-seq and ribosome-profiling assays
- Integration of GRO-seq, RNA-seq, and ribosome-profiling data
- Meta-analysis of GRO-seq data
- ChIP-seq assay
- Pearson Coefficient Correlation of histone marks
- Clustering of chromatin profiles
- Similarity analyses of proximities and distances
- Super-enhancer analysis by ROSE
- PageRank motif analysis
- HOMER motif analysis
- Analysis of GRO-seq density around ChIP-seq peaks
- Gene ontology analysis
- Western blotting and quantitative real-time PCR (qRT-PCR)
- Immunofluorescent imaging
- Fluorescence-activated cell sorting (FACS) analysis by flow cytometry
- RNA-seq of fixed cells after FACS sorting

● QUANTIFICATION AND STATISTICAL ANALYSIS

● DATA AND CODE AVAILABILITY

SUPPLEMENTAL INFORMATION

Supplemental Information can be found online at <https://doi.org/10.1016/j.celrep.2020.107532>.

ACKNOWLEDGMENTS

We thank Dr. Geoff Rosenfeld and members of his lab for providing a nurtured environment to develop this project. We also thank Dr. K. Jepsen (Director of the Institute of Genomic Medicine, UCSD) for sequencing support. S.J.N. is a recipient of a postdoctoral fellowship from the American Heart Association (14POST19860025) and a K01-NIDKK awardee (1K01DK121871). Q.M. is supported by a Postdoctoral Fellowship Award from the American Cancer Society (ACS). F.Y. is supported by the Ruth L. Kirschstein National Research Service Award from NIH. This work has been supported by funding provided to I.G.-B. from the U.S. Department of Defense (Pilot Award, W81XWH-14-1-0089; and Idea Award, W81XWH-12-1-0358), and the Ovarian Cancer Research Alliance (OCRA, Liz Tilberis Early Career Award, OC130397) bequest from the Estate of Agatha Pepper Fort.

AUTHOR CONTRIBUTIONS

Conceptualization, I.G.-B., A.A.-Q., and D.W. Supervision, Project Administration, and Funding Acquisition, I.G.-B. Investigation, F.Y., C.M., R.S.J., S.O., C.J., S.J.N., W.M., S.A., A.A.-Q., and I.G.-B. Formal Analysis and Visualization, Q.M., D.M., and I.G.-B. Writing – Original Draft, I.G.-B. and A.A.Q. Writing – Review & Editing, F.Y., R.S.J., S.J.N., D.W., A.A.-Q., and I.G.-B.

DECLARATION OF INTERESTS

The authors declare no competing interests.

Received: June 18, 2019

Revised: January 7, 2020

Accepted: March 27, 2020

Published: April 21, 2020

SUPPORTING CITATIONS

The following reference appears in the Supplemental Information: Allen et al. (2014).

REFERENCES

- Allen, M.A., Andrysiak, Z., Dengler, V.L., Mellert, H.S., Guarneri, A., Freeman, J.A., Sullivan, K.D., Galbraith, M.D., Luo, X., Kraus, W.L., et al. (2014). Global analysis of p53-regulated transcription identifies its direct targets and unexpected regulatory mechanisms. *eLife* 3, e02200.
- Almenar-Queralt, A., Kim, S.N., Benner, C., Herrera, C.M., Kang, D.E., Garcia-Bassets, I., and Goldstein, L.S.B. (2013). Presenilins regulate neutrophilic gene expression and neutrophil-dependent agrin cleavage via cyclic AMP response element-binding protein (CREB) modulation. *J. Biol. Chem.* 288, 35222–35236.
- Almenar-Queralt, A., Merkurjev, D., Kim, H.S., Navarro, M., Ma, Q., Chaves, R.S., Allegue, C., Driscoll, S.P., Chen, A.G., Kohlhofer, B., et al. (2019). Chromatin establishes an immature version of neuronal protocadherin selection during the naive-to-primed conversion of pluripotent stem cells. *Nat. Genet.* 51, 1691–1701.
- Ando, K., Shioda, S., Handa, H., and Kataoka, K. (2003). Isolation and characterization of an alternatively spliced variant of transcription factor Islet-1. *J. Mol. Endocrinol.* 31, 419–425.
- Andorfer, P., Heuwieser, A., Heinzel, A., Lukas, A., Mayer, B., and Perco, P. (2016). Vascular endothelial growth factor A as predictive marker for mTOR inhibition in relapsing high-grade serous ovarian cancer. *BMC Syst. Biol.* 10, 33.
- Ang, W.H., Myint, M., and Lippard, S.J. (2010). Transcription inhibition by platinum-DNA cross-links in live mammalian cells. *J. Am. Chem. Soc.* 132, 7429–7435.
- Anglesio, M.S., Wiegand, K.C., Melnyk, N., Chow, C., Salamanca, C., Prentice, L.M., Senz, J., Yang, W., Spillman, M.A., Cochrane, D.R., et al. (2013). Type-specific cell line models for type-specific ovarian cancer research. *PLoS One* 8, e72162.
- Bao, J., Li, M., Liang, S., Yang, Y., Wu, J., Zou, Q., Fang, S., Chen, S., and Guo, L. (2019). Integrated high-throughput analysis identifies super enhancers associated with chemoresistance in SCLC. *BMC Med. Genomics* 12, 67.
- Barzelay, A., Hochhauser, E., Entin-Meer, M., Chepurko, Y., Birk, E., Afek, A., Barshack, I., Pinhas, L., Rivo, Y., Ben-Shoshan, J., et al. (2012). Islet-1 gene delivery improves myocardial performance after experimental infarction. *Atherosclerosis* 223, 284–290.
- Bass, A.J., Watanabe, H., Mermel, C.H., Yu, S., Perner, S., Verhaak, R.G., Kim, S.Y., Wardwell, L., Tamayo, P., Gat-Viks, I., et al. (2009). SOX2 is an amplified lineage-survival oncogene in lung and esophageal squamous cell carcinomas. *Nat. Genet.* 41, 1238–1242.
- Beaufort, C.M., Helmijr, J.C.A., Piskorz, A.M., Hoogstraat, M., Ruigrok-Ritstier, K., Besselink, N., Murtaza, M., van IJcken, W.F.J., Heine, A.A.J., Smid, M., et al. (2014). Ovarian cancer cell line panel (OCCP): clinical importance of in vitro morphological subtypes. *PLoS One* 9, e103988.
- Becker, J.P., Weiss, J., and Theile, D. (2014). Cisplatin, oxaliplatin, and carboplatin unequally inhibit *in vitro* mRNA translation. *Toxicol. Lett.* 225, 43–47.
- Benner, C., Konovalov, S., Mackintosh, C., Hutt, K.R., Stunnenberg, R., and Garcia-Bassets, I. (2013). Decoding a signature-based model of transcription cofactor recruitment dictated by cardinal cis-regulatory elements in proximal promoter regions. *PLoS Genet.* 9, e1003906.
- Bortner, C.D., and Cidlowski, J.A. (2003). Uncoupling cell shrinkage from apoptosis reveals that Na⁺ influx is required for volume loss during programmed cell death. *J. Biol. Chem.* 278, 39176–39184.
- Bradner, J.E., Hnisz, D., and Young, R.A. (2017). Transcriptional Addiction in Cancer. *Cell* 168, 629–643.
- Butler, A., Hoffman, P., Smibert, P., Papalex, E., and Satija, R. (2018). Integrating single-cell transcriptomic data across different conditions, technologies, and species. *Nat. Biotechnol.* 36, 411–420.

- Chepelev, I., Wei, G., Wangsa, D., Tang, Q., and Zhao, K. (2012). Characterization of genome-wide enhancer-promoter interactions reveals co-expression of interacting genes and modes of higher order chromatin organization. *Cell Res.* 22, 490–503.
- Ching, S.T., Infante, C.R., Du, W., Sharir, A., Park, S., Menke, D.B., and Klein, O.D. (2018). *Isl1* mediates mesenchymal expansion in the developing external genitalia via regulation of *Bmp4*, *Fgf10* and *Wnt5a*. *Hum. Mol. Genet.* 27, 107–119.
- Damia, G., and Broggini, M. (2019). Platinum Resistance in Ovarian Cancer: Role of DNA Repair. *Cancers (Basel)* 11, E119.
- Dekker, J., Marti-Renom, M.A., and Mirny, L.A. (2013). Exploring the three-dimensional organization of genomes: interpreting chromatin interaction data. *Nat. Rev. Genet.* 14, 390–403.
- Di Veroli, G.Y., Fornari, C., Goldlust, I., Mills, G., Koh, S.B., Bramhall, J.L., Richards, F.M., and Jodrell, D.I. (2015). An automated fitting procedure and software for dose-response curves with multiphasic features. *Sci. Rep.* 5, 14701.
- Domcke, S., Sinha, R., Levine, D.A., Sander, C., and Schultz, N. (2013). Evaluating cell lines as tumour models by comparison of genomic profiles. *Nat. Commun.* 4, 2126.
- Easwaran, H., Tsai, H.-C., and Baylin, S.B. (2014). Cancer epigenetics: tumor heterogeneity, plasticity of stem-like states, and drug resistance. *Mol. Cell* 54, 716–727.
- ENCODE Project Consortium (2012). An integrated encyclopedia of DNA elements in the human genome. *Nature* 489, 57–74.
- Fang, Y., Zhang, C., Wu, T., Wang, Q., Liu, J., and Dai, P. (2017). Transcriptome Sequencing Reveals Key Pathways and Genes Associated with Cisplatin Resistance in Lung Adenocarcinoma A549 Cells. *PLoS One* 12, e0170609.
- Fei, T., Li, W., Peng, J., Xiao, T., Chen, C.-H., Wu, A., Huang, J., Zang, C., Liu, X.S., and Brown, M. (2019). Deciphering essential cistromes using genome-wide CRISPR screens. *Proc. Natl. Acad. Sci. USA* 116, 25186–25195.
- Flavahan, W.A., Gaskell, E., and Bernstein, B.E. (2017). Epigenetic plasticity and the hallmarks of cancer. *Science* 357, eaal2380.
- Fulco, C.P., Nasser, J., Jones, T.R., Munson, G., Bergman, D.T., Subramanian, V., Grossman, S.R., Anyoha, R., Doughty, B.R., Patwardhan, T.A., et al. (2019). Activity-by-contact model of enhancer-promoter regulation from thousands of CRISPR perturbations. *Nat. Genet.* 51, 1664–1669.
- Garcia-Bassets, I., and Wang, D. (2012). Cistrome plasticity and mechanisms of cistrome reprogramming. *Cell Cycle* 11, 3199–3210.
- Garraway, L.A., Widlund, H.R., Rubin, M.A., Getz, G., Berger, A.J., Ramaswamy, S., Beroukhim, R., Milner, D.A., Granter, S.R., Du, J., et al. (2005). Integrative genomic analyses identify MITF as a lineage survival oncogene amplified in malignant melanoma. *Nature* 436, 117–122.
- Gong, Y.-N., Crawford, J.C., Heckmann, B.L., and Green, D.R. (2019). To the edge of cell death and back. *FEBS J.* 286, 430–440.
- Gudipaty, S.A., Conner, C.M., Rosenblatt, J., and Montell, D.J. (2018). Unconventional Ways to Live and Die: Cell Death and Survival in Development, Homeostasis, and Disease. *Annu. Rev. Cell Dev. Biol.* 34, 311–332.
- Harder, H.C., and Rosenberg, B. (1970). Inhibitory effects of anti-tumor platinum compounds on DNA, RNA and protein syntheses in mammalian cells in vitro. *Int. J. Cancer* 6, 207–216.
- Hawkins, R.D., Hon, G.C., Yang, C., Antosiewicz-Bourget, J.E., Lee, L.K., Ngo, Q.-M., Klugman, S., Ching, K.A., Edsall, L.E., Ye, Z., et al. (2011). Dynamic chromatin states in human ES cells reveal potential regulatory sequences and genes involved in pluripotency. *Cell Res.* 21, 1393–1409.
- Heinz, S., Benner, C., Spann, N., Bertolino, E., Lin, Y.C., Laslo, P., Cheng, J.X., Murre, C., Singh, H., and Glass, C.K. (2010). Simple combinations of lineage-determining transcription factors prime cis-regulatory elements required for macrophage and B cell identities. *Mol. Cell* 38, 576–589.
- Helleman, J., Jansen, M.P.H.M., Span, P.N., van Staveren, I.L., Massuger, L.F.A.G., Meijer-van Gelder, M.E., Sweep, F.C.G.J., Ewing, P.C., van der Burg, M.E.L., Stoter, G., et al. (2006). Molecular profiling of platinum resistant ovarian cancer. *Int. J. Cancer* 118, 1963–1971.
- Heminger, K.A., Hartson, S.D., Rogers, J., and Matts, R.L. (1997). Cisplatin inhibits protein synthesis in rabbit reticulocyte lysate by causing an arrest in elongation. *Arch. Biochem. Biophys.* 344, 200–207.
- Hnisz, D., Abraham, B.J., Lee, T.I., Lau, A., Saint-André, V., Sigova, A.A., Hoke, H.A., and Young, R.A. (2013). Super-enhancers in the control of cell identity and disease. *Cell* 155, 934–947.
- Holohan, C., Van Schaeybroeck, S., Longley, D.B., and Johnston, P.G. (2013). Cancer drug resistance: an evolving paradigm. *Nat. Rev. Cancer* 13, 714–726.
- Hrvatin, S., Deng, F., O'Donnell, C.W., Gifford, D.K., and Melton, D.A. (2014). MARIS: method for analyzing RNA following intracellular sorting. *PLoS One* 9, e89459.
- Hu, J., Lieb, J.D., Sancar, A., and Adar, S. (2016). Cisplatin DNA damage and repair maps of the human genome at single-nucleotide resolution. *Proc. Natl. Acad. Sci. USA* 113, 11507–11512.
- Huang, M., Kantardzhieva, A., Scheffer, D., Liberman, M.C., and Chen, Z.-Y. (2013). Hair cell overexpression of *Isl1* reduces age-related and noise-induced hearing loss. *J. Neurosci.* 33, 15086–15094.
- Ince, T.A., Sousa, A.D., Jones, M.A., Harrell, J.C., Agoston, E.S., Krohn, M., Selfors, L.M., Liu, W., Chen, K., Yong, M., et al. (2015). Characterization of twenty-five ovarian tumour cell lines that phenocopy primary tumours. *Nat. Commun.* 6, 7419.
- Kim, Y.-J., Yoon, H.-Y., Kim, J.S., Kang, H.W., Min, B.-D., Kim, S.-K., Ha, Y.-S., Kim, I.Y., Ryu, K.H., Lee, S.-C., and Kim, W.J. (2013). HOXA9, *ISL1* and ALDH1A3 methylation patterns as prognostic markers for nonmuscle invasive bladder cancer: array-based DNA methylation and expression profiling. *Int. J. Cancer* 133, 1135–1142.
- Knoechel, B., Roderick, J.E., Williamson, K.E., Zhu, J., Lohr, J.G., Cotton, M.J., Gillespie, S.M., Fernandez, D., Ku, M., Wang, H., et al. (2014). An epigenetic mechanism of resistance to targeted therapy in T cell acute lymphoblastic leukemia. *Nat. Genet.* 46, 364–370.
- Koche, R.P., Smith, Z.D., Adli, M., Gu, H., Ku, M., Gnirke, A., Bernstein, B.E., and Meissner, A. (2011). Reprogramming factor expression initiates widespread targeted chromatin remodeling. *Cell Stem Cell* 8, 96–105.
- Konermann, S., Brigham, M.D., Trevino, A.E., Joung, J., Abudayyeh, O.O., Barcena, C., Hsu, P.D., Habib, N., Gootenberg, J.S., Nishimasu, H., et al. (2015). Genome-scale transcriptional activation by an engineered CRISPR-Cas9 complex. *Nature* 517, 583–588.
- Konovalov, S., and Garcia-Bassets, I. (2013). Analysis of the levels of lysine-specific demethylase 1 (LSD1) mRNA in human ovarian tumors and the effects of chemical LSD1 inhibitors in ovarian cancer cell lines. *J. Ovarian Res.* 6, 75.
- Koppikar, P., Bhagwat, N., Kilpivaara, O., Manshouri, T., Adli, M., Hricik, T., Liu, F., Saunders, L.M., Mullally, A., Abdel-Wahab, O., et al. (2012). Heterodimeric JAK-STAT activation as a mechanism of persistence to JAK2 inhibitor therapy. *Nature* 489, 155–159.
- Li, M., Balch, C., Montgomery, J.S., Jeong, M., Chung, J.H., Yan, P., Huang, T.H.M., Kim, S., and Nephew, K.P. (2009). Integrated analysis of DNA methylation and gene expression reveals specific signaling pathways associated with platinum resistance in ovarian cancer. *BMC Med. Genomics* 2, 34.
- Li, Y., Pan, J., Wei, C., Chen, J., Liu, Y., Liu, J., Zhang, X., Evans, S.M., Cui, Y., and Cui, S. (2014). LIM homeodomain transcription factor *Isl1* directs normal pyloric development by targeting *Gata3*. *BMC Biol.* 12, 25.
- Li, Y., Tian, S., Lei, I., Liu, L., Ma, P., and Wang, Z. (2017). Transplantation of multipotent *Isl1*+ cardiac progenitor cells preserves infarcted heart function in mice. *Am. J. Transl. Res.* 9, 1530–1542.
- Liang, X., Song, M.-R., Xu, Z., Lanuza, G.M., Liu, Y., Zhuang, T., Chen, Y., Pfaff, S.L., Evans, S.M., and Sun, Y. (2011). *Isl1* is required for multiple aspects of motor neuron development. *Mol. Cell. Neurosci.* 47, 215–222.
- Liau, B.B., Sievers, C., Donohue, L.K., Gillespie, S.M., Flavahan, W.A., Miller, T.E., Venteicher, A.S., Hebert, C.H., Carey, C.D., Rodig, S.J., et al. (2017). Adaptive Chromatin Remodeling Drives Glioblastoma Stem Cell Plasticity and Drug Tolerance. *Cell Stem Cell* 20, 233–246.e7.
- Liu, J., Li, W., Wang, Y., Fan, W., Li, P., Lin, W., Yang, D., Fang, R., Feng, M., Hu, C., et al. (2014). *Isl1*-overexpression in human mesenchymal stem cells

- promotes vascularization through monocyte chemoattractant protein-3. *Stem Cells* 32, 1843–1854.
- Lloyd, K.L., Cree, I.A., and Savage, R.S. (2015). Prediction of resistance to chemotherapy in ovarian cancer: a systematic review. *BMC Cancer* 15, 117.
- Lovén, J., Hoke, H.A., Lin, C.Y., Lau, A., Orlando, D.A., Vakoc, C.R., Bradner, J.E., Lee, T.I., and Young, R.A. (2013). Selective inhibition of tumor oncogenes by disruption of super-enhancers. *Cell* 153, 320–334.
- Lu, K.-M., Evans, S.M., Hirano, S., and Liu, F.-C. (2014). Dual role for Islet-1 in promoting striatonigral and repressing striatopallidal genetic programs to specify striatonigral cell identity. *Proc. Natl. Acad. Sci. USA* 111, E168–E177.
- Mansoori, B., Mohammadi, A., Davudian, S., Shirjang, S., and Baradaran, B. (2017). The Different Mechanisms of Cancer Drug Resistance: A Brief Review. *Adv. Pharm. Bull.* 7, 339–348.
- Marissen, W.E., and Lloyd, R.E. (1998). Eukaryotic translation initiation factor 4G is targeted for proteolytic cleavage by caspase 3 during inhibition of translation in apoptotic cells. *Mol. Cell. Biol.* 18, 7565–7574.
- Melnikov, S.V., Söll, D., Steitz, T.A., and Polikanov, Y.S. (2016). Insights into RNA binding by the anticancer drug cisplatin from the crystal structure of cisplatin-modified ribosome. *Nucleic Acids Res.* 44, 4978–4987.
- Mikkelsen, T.S., Ku, M., Jaffe, D.B., Issac, B., Lieberman, E., Giannoukos, G., Alvarez, P., Brockman, W., Kim, T.-K., Koche, R.P., et al. (2007). Genome-wide maps of chromatin state in pluripotent and lineage-committed cells. *Nature* 448, 553–560.
- Mumbach, M.R., Satpathy, A.T., Boyle, E.A., Dai, C., Gowen, B.G., Cho, S.W., Nguyen, M.L., Rubin, A.J., Granja, J.M., Kazane, K.R., et al. (2017). Enhancer connectome in primary human cells identifies target genes of disease-associated DNA elements. *Nat. Genet.* 49, 1602–1612.
- Pan, L., Deng, M., Xie, X., and Gan, L. (2008). ISL1 and BRN3B co-regulate the differentiation of murine retinal ganglion cells. *Development* 135, 1981–1990.
- Pathania, R., Ramachandran, S., Elangovan, S., Padia, R., Yang, P., Cinghu, S., Veeranan-Karmegam, R., Arjunan, P., Gnana-Prakasam, J.P., Sadanand, F., et al. (2015). DNMT1 is essential for mammary and cancer stem cell maintenance and tumorigenesis. *Nat. Commun.* 6, 6910.
- Raudenska, M., Balvan, J., Fojtu, M., Gumulec, J., and Masarik, M. (2019). Unexpected therapeutic effects of cisplatin. *Metalomics* 11, 1182–1199.
- Roesch, A., Vultur, A., Bogeski, I., Wang, H., Zimmermann, K.M., Speicher, D., Körbel, C., Laschke, M.W., Gimotty, P.A., Philipp, S.E., et al. (2013). Overcoming intrinsic multidrug resistance in melanoma by blocking the mitochondrial respiratory chain of slow-cycling JARID1B(high) cells. *Cancer Cell* 23, 811–825.
- Ron, G., Globerson, Y., Moran, D., and Kaplan, T. (2017). Promoter-enhancer interactions identified from Hi-C data using probabilistic models and hierarchical topological domains. *Nat. Commun.* 8, 2237.
- Rosenberg, J.M., and Sato, P.H. (1993). Cisplatin inhibits in vitro translation by preventing the formation of complete initiation complex. *Mol. Pharmacol.* 43, 491–497.
- Rusan, M., Li, K., Li, Y., Christensen, C.L., Abraham, B.J., Kwiatkowski, N., Buczkowski, K.A., Bockorny, B., Chen, T., Li, S., et al. (2018). Suppression of Adaptive Responses to Targeted Cancer Therapy by Transcriptional Repression. *Cancer Discov.* 8, 59–73.
- Salari, K., Spulak, M.E., Cuff, J., Forster, A.D., Giacomini, C.P., Huang, S., Ko, M.E., Lin, A.Y., van de Rijn, M., and Pollack, J.R. (2012). CDX2 is an amplified lineage-survival oncogene in colorectal cancer. *Proc. Natl. Acad. Sci. USA* 109, E3196–E3205.
- Salgia, R., and Kulkarni, P. (2018). The Genetic/Non-genetic Duality of Drug “Resistance” in Cancer. *Trends Cancer* 4, 110–118.
- Sato, P.H., Rosenberg, J.M., and Sato, R.I. (1996). Differences in the inhibition of translation by cisplatin, transplatin, and certain related compounds. *Biochem. Pharmacol.* 52, 1895–1902.
- Sengupta, S., and George, R.E. (2017). Super-Enhancer-Driven Transcriptional Dependencies in Cancer. *Trends Cancer* 3, 269–281.
- Shaffer, S.M., Dunagin, M.C., Torborg, S.R., Torre, E.A., Emert, B., Krepler, C., Begiri, M., Sproesser, K., Brafford, P.A., Xiao, M., et al. (2017). Rare cell variability and drug-induced reprogramming as a mode of cancer drug resistance. *Nature* 546, 431–435.
- Sharma, S.V., Lee, D.Y., Li, B., Quinlan, M.P., Takahashi, F., Maheswaran, S., McDermott, U., Azizian, N., Zou, L., Fischbach, M.A., et al. (2010). A chromatin-mediated reversible drug-tolerant state in cancer cell subpopulations. *Cell* 141, 69–80.
- Shen, D.-W., Pouliot, L.M., Hall, M.D., and Gottesman, M.M. (2012). Cisplatin resistance: a cellular self-defense mechanism resulting from multiple epigenetic and genetic changes. *Pharmacol. Rev.* 64, 706–721.
- Solár, P., and Sytkowski, A.J. (2011). Differentially expressed genes associated with cisplatin resistance in human ovarian adenocarcinoma cell line A2780. *Cancer Lett.* 309, 11–18.
- Sun, Y., Dykes, I.M., Liang, X., Eng, S.R., Evans, S.M., and Turner, E.E. (2008). A central role for Islet1 in sensory neuron development linking sensory and spinal gene regulatory programs. *Nat. Neurosci.* 11, 1283–1293.
- Tang, H.M., and Tang, H.L. (2018). Anastasis: recovery from the brink of cell death. *R. Soc. Open Sci.* 5, 180442.
- Teng, S., Li, Y.E., Yang, M., Qi, R., Huang, Y., Wang, Q., Zhang, Y., Chen, S., Li, S., Lin, K., et al. (2019). Tissue-specific transcription reprogramming promotes liver metastasis of colorectal cancer. *Cell Res.* 30, 34–49.
- Verhaak, R.G.W., Tamayo, P., Yang, J.-Y., Hubbard, D., Zhang, H., Creighton, C.J., Fereday, S., Lawrence, M., Carter, S.L., Mermel, C.H., et al.; Cancer Genome Atlas Research Network (2013). Prognostically relevant gene signatures of high-grade serous ovarian carcinoma. *J. Clin. Invest.* 123, 517–525.
- Wang, D., Garcia-Bassets, I., Benner, C., Li, W., Su, X., Zhou, Y., Qiu, J., Liu, W., Kaikkonen, M.U., Ohgi, K.A., et al. (2011). Reprogramming transcription by distinct classes of enhancers functionally defined by eRNA. *Nature* 474, 390–394.
- Weir, B.A., Woo, M.S., Getz, G., Perner, S., Ding, L., Beroukhim, R., Lin, W.M., Province, M.A., Kraja, A., Johnson, L.A., et al. (2007). Characterizing the cancer genome in lung adenocarcinoma. *Nature* 450, 893–898.
- Whyte, W.A., Orlando, D.A., Hnisz, D., Abraham, B.J., Lin, C.Y., Kagey, M.H., Rahl, P.B., Lee, T.I., and Young, R.A. (2013). Master transcription factors and mediator establish super-enhancers at key cell identity genes. *Cell* 153, 307–319.
- Xiang, Q., Liao, Y., Chao, H., Huang, W., Liu, J., Chen, H., Hong, D., Zou, Z., Xiang, A.P., and Li, W. (2018). ISL1 overexpression enhances the survival of transplanted human mesenchymal stem cells in a murine myocardial infarction model. *Stem Cell Res. Ther.* 9, 51.
- Xie, S., Duan, J., Li, B., Zhou, P., and Hon, G.C. (2017). Multiplexed Engineering and Analysis of Combinatorial Enhancer Activity in Single Cells. *Mol. Cell* 66, 285–299.e5.
- Yu, B., Zhang, K., Milner, J.J., Toma, C., Chen, R., Scott-Browne, J.P., Pereira, R.M., Crotty, S., Chang, J.T., Pipkin, M.E., et al. (2017). Epigenetic landscapes reveal transcription factors that regulate CD8⁺ T cell differentiation. *Nat. Immunol.* 18, 573–582.
- Zeller, C., Dai, W., Steele, N.L., Siddiq, A., Walley, A.J., Wilhelm-Benartzi, C.S.M., Rizzo, S., van der Zee, A., Plumb, J.A., and Brown, R. (2012). Candidate DNA methylation drivers of acquired cisplatin resistance in ovarian cancer identified by methylome and expression profiling. *Oncogene* 31, 4567–4576.
- Zhang, J.A., Mortazavi, A., Williams, B.A., Wold, B.J., and Rothenberg, E.V. (2012). Dynamic transformations of genome-wide epigenetic marking and transcriptional control establish T cell identity. *Cell* 149, 467–482.
- Zhang, Y., Wang, L., Gao, P., Sun, Z., Li, N., Lu, Y., Shen, J., Sun, J., Yang, Y., Dai, H., and Cai, H. (2018). ISL1 promotes cancer progression and inhibits cisplatin sensitivity in triple-negative breast cancer cells. *Int. J. Mol. Med.* 42, 2343–2352.

STAR★METHODS

KEY RESOURCES TABLE

REAGENT or RESOURCE	SOURCE	IDENTIFIER
Antibodies		
Anti-BrdU (IIB5) AC agarose	Santa Cruz Antibodies	Cat#sc-32323 AC
Anti-H3K4me3	Millipore	Cat#07-473; RRID:AB_1977252
Anti-H3K4me2	Active Motif	Cat#39141; RRID:AB_2614985
Anti-H3K27ac	Abcam	Cat#ab4729; RRID:AB_2118291
Anti-p53	Active Motif	Cat#39334; RRID:AB_2753148
Anti-ISL1	DHSB	Cat#39.4D5 s; RRID:AB_2314683
Anti-EGR1	Santa Cruz Biotechnology	Cat#sc-110; RRID:AB_2097174
Anti-CTCF antibody	Active Motif	Cat#61932; RRID:AB_2614975
Anti-mouse Alexa Fluor-488, donkey	Life Technologies	Cat#A21202; RRID:AB_141607
Chemicals and Reagents		
Cisplatin	Sigma-Aldrich	Cat#P4394
Poly-D-lysine	Sigma-Aldrich	Cat#P7280
N,N-dimethylformamide	Sigma-Aldrich	Cat#227056
Vectashield Mounting media	Vector Laboratories	Cat#H-1000
RNasin Recombinant Inhibitor	Promega	Cat#N2515
AMPure XP	Beckman Coulter	Cat#A63881
Formaldehyde	Sigma-Aldrich	Cat#F8775
Paraformaldehyde	Electron Microscopy Sciences	Cat#15710
Triton X-100	Sigma-Aldrich	Cat#T8787
Tween 20	Sigma-Aldrich	Cat#P9416
DAPI	Sigma-Aldrich	Cat#D9542
EDTA	Invitrogen	Cat#15575020
HEPES	GIBCO	Cat#15630080
RPMI-1640-Glutamax I	Life Technologies	Cat#61870-036
DMEM-Glutamax I	GIBCO	Cat#10566-016
Fetal bovine serum	Omega Scientific	Cat#FB-11
Penicillin-streptomycin solution	Gemini Bio	Cat#400-109
Blasticidin S HCl	GIBCO	Cat#A1113903
Puromycin	GIBCO	Cat#A11138-03
Trypsin EDTA	GIBCO	Cat#25200056
PBS	GIBCO	Cat#10010023
Critical Commercial Assays		
RecoverAll Total Nucleic Acid Isolation kit	Thermo Fisher Scientific	Cat#AM1975
ARTseq Ribosome Profiling kit	Epicenter	Cat#RPHMR12126
TruSeq Stranded mRNA LT kit	Illumina	Cat# 20020594
KAPA LTP Library Preparation Kit	Kapa BioSystems	Cat#KK8232
CellTiter 96 AQueous Nonradioactive Cell Proliferation Assay	Promega	Cat#G5421
Deposited Data		
Raw and analyzed data	This paper	GSE129702
ChIP-seq data for H3K27ac in A549 cells	(ENCODE Project Consortium, 2012)	GSM1003578
RNA-seq in A549 and A549cis cells	(Fang et al., 2017)	SRP087614

(Continued on next page)

Continued

REAGENT or RESOURCE	SOURCE	IDENTIFIER
RNA-seq cancer lines	Depmap	RRID:SCR_017655
RNA-seq data in cancer samples	cBioPortal	RRID:SCR_014555
RNA-seq data in normal tissues	GTEX Analysis	RRID:SCR_001618
Experimental Models: Cell Lines		
Human A2780	Sigma-Aldrich	Cat#93112519; RRID:CVCL_0134
Human A2780cis	Sigma-Aldrich	Cat#93112517; RRID:CVCL_1942
Human A549	Laboratory of Robert Schooley	RRID:CVCL_0023
Human HEK293T	Laboratory of Michael Rosenfeld	RRID:CVCL_0063
Oligonucleotides		
gRNA #1 targeting sequence 5', TCTCCCGCTGGCTGCCGAG	This paper	N/A
gRNA #1 targeting sequence 3', CCAACCTCGCCGGCTTAAAT	This paper	N/A
gRNA #2 targeting sequence 5', GGCCGTTCTCCCCCGAAGCT	This paper	N/A
gRNA #2 targeting sequence 3', CTCCTAGATCCGCGAGGGCG	This paper	N/A
ISL1 expression 5' GCGGCAATCAGATTACGAT	This paper	N/A
ISL1 expression 3' GCGCATTGATCCCGTACAA	This paper	N/A
Recombinant DNA		
Lenti-dCas9-KRAB-Blast	Addgene	Cat#89567; RRID:Addgene_89567
Lenti dCAS-VP64-Blast	Addgene	Cat#61425; RRID:Addgene_61425
pLKO.1-U6-2sgRNA-ccdb-EF1a-Puro	Laboratory of Xingxu Huang	N/A
psPAX2	Addgene	Cat#12260; RRID:Addgene_12260
pMD2.G	Addgene	Cat#12259; RRID:Addgene_12259
Software and Algorithms		
CRISPR Design	ChopChop	RRID:SCR_015723
Bowtie 1.1.2	Bowtie	RRID:SCR_005476
HOMER	Benner Lab	RRID:SCR_010881
KMC	N/A	http://home.cc.umanitoba.ca/~psgndb/birchomedir/doc/MeV/manual/KMC.html
FOM	N/A	http://home.cc.umanitoba.ca/~psgndb/birchomedir/doc/MeV/manual/FOM.html
MeV	MeV	http://mev.tm4.org/#/welcome
UCSC Genome Browser	UCSC	RRID:SCR_005780
R	R Project	https://www.r-project.org/
EdgR	N/A	http://www.bioconductor.org/packages/release/bioc/html/edgeR.html
Seurat pipeline	Satja Lab	RRID:SCR_016341
ROSE	Young Lab	RRID:SCR_017390
PageRank	Kai Zhang/Wei Wang Lab	https://github.com/kaizhang/Taiji
WebLOGO	WebLOGO	RRID:SCR_010236
DAVID	DAVID	RRID:SCR_001881
Dr. Fit	(Di Veroli et al., 2015)	https://sourceforge.net/projects/drfit/
FlowJo 7.6.3 Software	FlowJo	RRID:SCR_008520

(Continued on next page)

Continued

REAGENT or RESOURCE	SOURCE	IDENTIFIER
ImageJ 1.51 s Software	ImageJ	RRID:SCR_003070
KC junior Software	BioTek	https://www.biotek.com
FACSDiva Software	BD Biosciences	RRID:SCR_001456
Excel for Mac Software	Microsoft	RRID:SCR_016137
Prism 6 Software	GraphPad	RRID:SCR_002798
Clustree	N/A	https://cran.r-project.org/web/packages/clustree/vignettes/clustree.html

LEAD CONTACT AND MATERIAL AVAILABILITY

The plasmids pLKO.1-U6-2sgRNA-ccdb-EF1a-Puro containing the gRNAs designed in this study are available from the Lead Contact, Dr. Ivan Garcia-Bassets (lbassets@health.ucsd.edu) upon completion of a materials transfer agreement.

EXPERIMENTAL MODEL AND SUBJECT DETAILS

The ovarian cancer A2780 cell line (Cat#93112519; RRID:CVCL_0134) and its derivative A2780cis subline (Cat#93112517; RRID:CVCL_1942) were purchased authenticated from Sigma-Aldrich. The treatment applied to A2780cis cells was described in the Sigma-Aldrich website as chronic exposure of the parent A27890 line to increasing concentrations of cisplatin. Both cell populations were cultured in RPMI-1640-Glutamax I (Life Technologies, Cat#61870-036) and 10% fetal bovine serum (FBS, Omega Scientific, Cat#FB-11) at 5% CO₂ 37°C, and sub-cultured at 1:5 to 1:6 dilutions after dissociation with 0.25% trypsin EDTA (GIBCO, Cat#25200056). Media was changed every other day, or daily when cells reached > 50%–60% confluence. The two populations were authenticated by STR analysis after the bulk of experimental work ended, using ATCC services (https://www.atcc.org/en/Services/Testing_Services/Cell.Authentication_Testing_Service.aspx). In this study, the cisplatin treatment (Sigma-Aldrich, Cat#P4394, dissolved in N,N-dimethylformamide, Cat#227056, prepared fresh every time) was continuously administered for 3 days, adding fresh media with drug at day 0 and day 2 day. Some treatments were limited to 2 days, as indicated, with only one round of drug administration. Doses: 2 µM for A2780 cells and 6 µM for A2780cis cells (which correspond to IC₅₀ after 3 days) unless otherwise indicated. The ‘recovery’ condition refers to regular media without drug after treatment (we have observed that survivor cells regain cell division a few days after the 2/3-day treatment ends, and the culture can be passaged normally again approximately 7-10 days later). The human lung adenocarcinoma A549 cell line (RRID:CVCL_0023) was a gift from Dr. Robert Schooley’s lab. A549 cells were cultured in Dulbecco’s modified Eagle’s-Glutamax I medium (DMEM-Glutamax I, GIBCO, Cat#10566-016) supplemented with 10% FBS (FBS, Omega Scientific, Cat#FB-11) and antibiotics penicillin and streptomycin (100 µg/mL, Gemini Bio, Cat#400-109). Cells were treated for 3 days (dose: 800 µM, which corresponded to IC₅₀ after 3 days).

METHOD DETAILS**Generation of CRISPRi- and CRISPRa-modified sublines**

To stably downregulate and upregulate *ISL1*-gene expression in A2780 and A2780cis cells, respectively, we used the following plasmids: Lenti-dCas9-KRAB-Blast (Addgene Cat#89567, RRID:Addgene_89567), a gift from Dr. Gary Hong ([Xie et al., 2017](#)); Lenti-dCAS-VP64_Blast (Addgene Cat#61425, RRID:Addgene_61425), a gift from Dr. Feng Zhang ([Konermann et al., 2015](#)); gRNA plasmid pLKO.1-U6-2sgRNA-ccdb-EF1a-Puro, a gift from Dr. Xingyu Huang (ShanghaiTech University, China); and the lentiviral packaging plasmids psPAX2 (Addgene Cat#12260, RRID:Addgene_12260) and pMD2.G (Addgene Cat#12259, RRID:Addgene_12259), gifts from Dr. Didier Trono. As gRNAs, the following two pairs of sequences (based on <https://chopchop.cbu.uib.no>; RRID:SCR_015723) were cloned in the gRNA plasmid through the Esp3I (BsmBI) site: pair 1, TCTCCCGCTGGCTGCCGAG and CCAACTCCGCCGCTTAAAT; and pair 2, GGCGCTTCTCCCCGAAGCT and CTCCTAGATCCGCGAGGGCG. These gRNAs target the *ISL1* promoter between the two main H3K4me3 peaks at the TSS. To generate viral particles, the plasmids dCAS-VP64_Blast, Lenti-dCas9-KRAB-Blast, pLKO.1-gRNA1, pLKO.1-gRNA2 were independently transfected in combination with psPAX2 and pMD2.G into HEK293T cells (RRID:CVCL_0063) at a ratio 3:2.2:0.75. Viral particles were prepared according to the standard packaging and transduction protocols provided by Addgene (<https://www.addgene.org/protocols/lentivirus-production/>). After 24 hours, viral particles were harvested and used for transduction. Cells were seeded in 6-well plates at the same time as viral particles were added, and after one day, fresh medium supplemented with antibiotics for selection was added (blasticidin S HCl, GIBCO, Cat#A1113903, at 30 µg/mL; puromycin, GIBCO, Cat#A11138-03, at 1 µg/mL). After 2 weeks of antibiotic selection, cells were ready for analysis. The CRISPRi/a-modified sublines were routinely cultured in plates pre-covered with Poly-D-lysine (Sigma-Aldrich, Cat#P7280) for robust attachment.

Cell viability assays and IC₅₀ calculations

Automatic cell counts were based on trypan-blue staining (1:2 dilutions) using the Countess™ II Automated Cell Counter (Thermo Fisher Scientific). Dose-response tests were based on the MTS/PMS assay using the microQuant plate reader (BioTek) as previously described with some modifications (Konovalov and Garcia-Bassets, 2013). Briefly, cells were seeded in 96-well plates at confluence to limit proliferative events (200,000 cells per well in 200 µL media; quantification based on trypan-blue staining); the next day, 180 µL of medium were replaced with fresh medium supplemented with the drug as indicated (adjusting with vehicle solution). The next day, 180 µL of media were replaced with 180 µL of fresh medium. The second day, 150 µL of medium were replaced with 30 µL medium supplemented with 20 µL of MTS/PMS solution (20:1, v:v; CellTiter 96 AQueous Nonradioactive Cell Proliferation Assay, Promega, Cat#G5421. MTS [3-(4,5-dimethylthiazol-2-yl)-5-(3-carboxymethoxyphenyl)-2-(4-sulfophenyl)-2H-tetrazolium, inner salt] and PMS (phenazine methosulfate). Plates were maintained in cell incubators at 37°C (5% CO₂) for approximately 3 hours, and 490 nm absorbance was measured in a microQuant plate reader and the KC junior Software (Biotek Instruments, <https://www.bioteck.com>). Biological replicates (n = 2) with six technical replicates each (n = 6) were analyzed. For IC₅₀ calculations and visualization we used Excel (Microsoft; RRID:SCR_016137) and Prism 6 (GraphPad; RRID:SCR_002798), respectively. Cells under vehicle conditions were used to determine 100% viability (C1). Wells without cells or at conditions in which no cells remained alive after treatment were used to determine 0% viability (C2). Viability percentage (C3) was calculated as: ((C3-C2)/(C1-C2)) * 100 in Excel. Cell viability graph show the average (mean) value of viable cells under each condition, ± s.e.m. After exporting these data to Prism 6, half maximum inhibitory concentration (IC₅₀, or best fit) values and 95% confidence intervals (95% CI) were then estimated by calculating the nonlinear regression (curve fit, dose response-inhibition variable slope) with Prism 6.

GRO-seq, RNA-seq and ribosome-profiling assays

We performed the GRO-seq assay exactly as previously described, starting with 1x10⁷ nuclei from a confluent 15 cm plate, and working with aliquots of 110 µL containing 5x10⁶ nuclei for each nuclear run-on assay (Wang et al., 2011). In order to immunopurify the Br-U RNA, we used 70 µL Anti-BrdU (IIB5) AC agarose beads (Santa Cruz Antibodies, Cat#sc-32323 AC). We performed RNA-seq and ribosome profiling using the ARTseq Ribosome Profiling kit and following the manufacturer's protocol (Epicenter, Cat#RPHMR12126) on cells harvested from a confluent 15 cm plate of cells (5–50 × 10⁶ cells). We processed 2–5 µg of total RNA for RNA-seq and a similar amount of ribosome-protected RNA for ribosome profiling. RNA integrity was examined using a TapeStation (Agilent Technologies). Libraries were generated using the Illumina TruSeq Stranded RNA LT kit (Illumina, Cat# 20020594) and following manufacturer's instructions and sequenced in an Illumina 2500 or 4000 instrument at the UCSD IGM Genomic Center. Genome browser tracks show tags or reads normalized to a sequencing depth of 10⁷ reads.

Integration of GRO-seq, RNA-seq, and ribosome-profiling data

Sequencing tags were aligned to hg18 Refseq database by using Bowtie2 (RRID:SCR_005476), allowing three tags per genomic location at most to get rid of spikes caused by particularly enriched regions (from rRNA and snoRNA transcripts in GRO-seq and, in general, for transcriptomic analyses, to eliminate potential issues derived from clonal amplification. We did not limit the number of reads in the GRO-seq analysis shown in Figure S5C. We have also repeated our analyses without limiting the number of tags per region for RNA-seq and ribosome-profiling, and at least 50% of the original dispersed genes were again dispersed genes without capping reads and the major conclusions could be replicated as most differences represented borderline cases of signal dispersion that can be included or excluded in the final list depending on the threshold and the parameters used. Calculations of gene transcription were based on the entire gene body for GRO-seq or on exonic regions only for RNA-seq and ribosome profiling using HOMER (RRID:SCR_010881). Tag counts were calculated strand specifically and plotted as described previously (Wang et al., 2011). The dispersed expression was calculated by using EdgR (<http://www.bioconductor.org/packages/release/bioc/html/edgeR.html>) with FDR < 0.001 and fold change (FC) > 1.5. For the t-SNE analysis, we applied by Seurat pipeline (RRID:SCR_016341). In particular, we used the V1.4 version in February 2018. The input matrix for t-SNE analysis in Seurat were generated from the list of n = 19,197 RefSeq protein-coding detected by GRO-seq, RNA-seq, and ribosome profiling separately, which is totally 12 parameters for each gene. A total of n = 6,136 reach certain threshold of detection in at least one of the 12 conditions (Seurat objective was initialized by keeping all genes expressed in > or = 1 condition, meanwhile keeping all conditions with at least 1 detected gene). Reads per kilo base of transcript per million mapped reads (RPKM) values with added 1 jitter value for each assay and condition were log transformed and scaled (out of gene region for GRO-seq, exons for RNA-seq, and cds for ribosome profiling. The conditions by gene matrix were imported as an 'Seurat' objective with parameter setting of "Setup" command as (min.cells = 1, min.genes = 1, is.expr = 1), and was filtered and calculated by using MeanVarPlot function (y.cutoff = 1, x.low.cutoff = 0, fxn.x = expMean, fxn.y = logVarDivMean). After the transformed 12 conditions by dispersed genes matrix was generated, we generated a SNN graph with clustering based on the Euclidean distance in the PCA space. We selected a resolution = 4 to maximize the clustering performance of the FindClusters() function in Seurat. This resolution resulted in the segregation of our multi-omic transcriptomic data into 17 modules. We note, however, that there might not be a 'perfect' number that can segregate modules maximizing clustering potential in some parts of the t-SNE plot without over-clustering in other parts of the plot—as most transcriptomic effects represent a continuum of values. For us, a good indicator that we choose an acceptable resolution is that, with a relatively large number of modules (17), most known p53 targets still accumulated in only one of them. During the revision, furthermore, we used an over-clustering tool, known as Clustree (<https://cran.r-project.org/web/packages/clustree/vignettes/clustree.html>), and compared the results of different

resolutions values (1, 2, 3, 4, 5, and 6). This test confirms that choosing the ‘right’ resolution is complex. We obtained 8, 10, 13, 17, 19, and 27 modules with the resolutions 1–6. Only a resolution of 2 compared to 1 does not result in nodes with multiple incoming edges, which indicates that the clustering does not break the data. Still, we note that the resolution of 4 is optimum in the sense that the ratio of number of nodes with multiple incoming edges relative to the number of modules is the lowest of the different resolutions tested. This result potentially indicates that this resolution might represent a good balance between maximizing the number of clusters and minimizing the number of over-clustering situations. In any case, we do not argue that resolutions other than 4 might also be acceptable. We think that every researcher should change this value according to the part of the t-SNE plot that represent the genes that focus his/her interest. For tSNE visualization, the top 12 dimensions of PCA results were selected as “pc.use” parameter in “Run-TSNE” command in Seurat, and the perplexity was set as 50 to get best separation of genes clusters on tSNE plot. The functions used above are referenced from the Seurat pipeline (https://satijalab.org/seurat/v1.4/pbmc3k_tutorial.html). We note that conducting the same analysis in which our study is based in **Figure 1D** (originally performed in February 2018) but using commands available in January 2020 for the V1.4 version provides virtually identical results (99.4% genes belong to the same modules) with the exception of five cases: NM_001195055 and NM_003670, which were originally part of M10, are moved to the neighbor M11 with 2020 commands; and NM_001288821, NM_002166, and NM_007254, which were originally part of M7, are moved to the neighbor M8 with 2020 commands. These genes are not highlighted in our study for any particular purpose and the main conclusions do not change as result of this 0.6% change in the t-SNE plot.

We calculated the Pearson correlation of dispersed gene expression comparing signal gene-by-gene of GRO-seq (X1–X4), RNA-seq (X5–X8), and ribosome profiling (X9–X12) data, in which X1/5/9 represent untreated A2780 cells, X2/6/10 represent 3-day-treated A2780 cells, X3/7/11 represent untreated A2780cis cells, and X4/8/12 represent 3-day-treated A2780cis cells. The average correlation is the following: GRO-seq versus RNA-seq, 0.33363839; GRO-seq versus ribosome profiling, 0.0547063; and, RNA-seq versus ribosome profiling, 0.69699331. RNA-seq and ribosome profiling correlations are fairly good, yet still far from ‘perfect’. GRO-seq data is clearly not correlated with the other two assays. By conditions, these are the numbers: X1 versus X5, 0.25383912; X2 versus X6, 0.27144426; X3 versus X7, 0.36563695; X4 versus X8, 0.44363323; X5 versus X9, 0.65546447; X6 versus X10, 0.69480447; X7 versus X11, 0.70764541; X8 versus X12, 0.73005888; X1 versus X9, 0.26797526; X2 versus X10, 0.19950626; X3 versus X11, 0.16752992; and, X4 versus X12, 0.24028939.

For clarity, for those who may try to replicate our analysis, we re-annotated the number given by the algorithm to every individual module in the t-SNE to follow a more intuitive logic: starting from the top and ending at the bottom and from the left to the right (see **Figure 1D**). The re-annotation is the following (the first number represents the annotation given by the algorithm; the second number represents the annotation that we generated): M1- > M2, M2- > M14, M3- > M15, M4- > M7, M5- > M13, M6- > M17, M7- > M1, M8- > M3, M9- > M9, M10- > M11, M11- > M8, M12- > M16, M13- > M12, M14- > M6, M15- > M10, M16- > M4, and M17- > M5. For the coloring of the t-SNE plots shown in **Figures 1E–1G** and **S1E–S1G**, we ranked all dispersed genes based on GRO-seq, RNA-seq, or ribosome profiling normalized signal in the indicated condition in **Figures 1E** and **S1E**, or based on fold change in the indicated comparisons: GRO-seq versus RNA-seq, GRO-seq versus ribosome profiling, or RNA-seq versus ribosome profiling signal in **Figures 1F** and **S1F**; or A2780 versus A2780cis signal in **Figures 1G** and **S1G**. We segregated the ranked genes into 9 groups of the same number of genes and represented each group with a different coloring tone as indicated in **Figures 1E** and **S1E**, or only the top-two groups with the same color in **Figures 1F** and **S1F** or the top-two groups with a different color in **Figures 1G** and **S1G** (red and dark blue represent the top group and orange and light blue represent the second group). In the two last cases, therefore, only 4 of the 9 groups are colored.

Meta-analysis of GRO-seq data

Meta-genes were generated, first, by assigning GRO-seq sequencing reads to the list of annotated human Refseq transcripts ($n = 27,782$, UCSC transcript list; RRID:SCR_005780). Then, we proceeded in two alternative manners. In one case (**Figures S2A** and **S5D**), we limited tag number per genomic position equal or less than 3 with the purpose to eliminate spikes coming from snoRNAs or rRNAs in intronic regions using the HOMER command (“analyzeRepeats.pl rna hg18 -noadj -strand + -count genes -pc 3 -condenseGenes -d Tag Directories”; RRID:SCR_010881). Then, we segregated the transcripts into the nine possible categories based on whether a transcript could be classified or not as differential expressed after 3 days of cisplatin treatment in either parental or pre-treated cells, or both [non: non-differentially expressed; up: upregulated; down: downregulated]: (in the order A2780 and A2780cis) non/non (1), up/up (2), down/down (3), up/non (4), down/non (5), non/up (6), non/down (7), up/down (8), and down/up (9). Out of the $n = 27,782$ transcripts, we identified $n = 1,739$ deferentially expressed ($FDR \leq 0.0001$, $FC \geq 0.58[\log_2 \text{based}]$ or $FC \leq -0.58[\log_2 \text{based}]$) using edgeR method called by HOMER (cmd = “getDiffExpression.pl Groseqgenes.txt -repeats control test -dispersion 0.0005 -edgeR”). Tag enrichment was normalized as a metagene based on the following regions: 3 kb upstream to TSS, gene body, and TTS to 5 kb downstream. The average tag enrichment profile plot was generated then using Excel based on each of the nine categories separately. Differential plots were generated as a subtraction of average tags for each of the indicated comparisons. Capping tags is a common practice in GRO-seq to eliminate super high-density signal derived from highly transcribed loci, such as those containing snoRNA and rRNA genes, that can interfere with overlapping signal from long transcriptional units containing introns encoding these short transcripts. To mitigate this effect, tag numbers per bp can be limited to 3. The caveat of this decision is that it may reduce the dynamic range of differential expression for the most highly expressed genes, although the dynamic range is relatively limited for most transcriptional units in GRO-seq and applying this limit should have no major effects on a global

scale. The second caveat, however, is highly relevant in our case. Capping tags may eliminate the possibility to assess transcriptional elongation blockage. In the second analysis (shown in Figure S2D), we therefore did not limit tag number per base (-pc < 0 >). These second set of meta-genes shows, as expected, spikes regardless of treatment but—we note—that regardless the presence of these spikes, the differential toward the 3' end of the meta-gene does not show evident changes between untreated and treated conditions, thus suggesting that transcription elongation is not affected by the drug. The spikes might be different in vehicle and cisplatin conditions, but likely as result of differential expression of short, highly expressed transcriptional units.

ChIP-seq assay

ChIPs were conducted as previously (Benner et al., 2013), using the following antibodies: H3K4me3 antibody (Millipore, Cat#07-473; RRID:AB_1977252), H3K4me2 antibody (Active Motif, Cat#39141; RRID:AB_2614985), H3K27ac antibody (Abcam, Cat#ab4729; RRID:AB_2118291), p53 antibody (Active Motif, Cat#39334; RRID:AB_2753148), ISL1 antibody (DHSB, Cat#39.4D5 s; RRID:AB_2314683), EGR1 antibody (Santa Cruz Biotechnology, Cat#sc-110; RRID:AB_2097174), and CTCF antibody (Active Motif, Cat#61932; RRID:AB_2614975). ChIP-seq libraries were prepared using the KAPA Library Preparation Kit (Cat#KK8232) and AMPure XP beads (Beckman Coulter, Cat#A63881) and sequenced on an Illumina 2500 or 4000 instruments. Sequencing tags were aligned to hg18 RefSeq database using Bowtie2. The ChIP-Seq peaks were identified by HOMER (<http://homer.ucsd.edu/homer/ngs/peaks.html>; RRID:SCR_010881). Given the different binding patterns of transcription factors and histone marks, HOMER parameters were optimized for the narrow tag distribution characteristic of transcription factors by searching for high read-enrichment regions within a 200-bp sliding window (findPeaks Histone Mark-ChIP-Seq/ -style factor -o auto -i Control-ChIP-Seq/). Regions of maximal density exceeding a given threshold were called as peaks, and adjacent peaks were set to be 500 bp away to avoid redundant detection. The threshold was set at false discovery rate (FDR) of 0.001 determined by peak finding using randomized tag positions in whole genome. For histone marks, we set “histone” as -style pattern (findPeaks Histone Mark-ChIP-Seq/ -style histone -o auto -i Control-ChIP-Seq/) and seed regions were initially found using a peak size of 500 bp (FDR = 0.001) to identify enriched loci. Enriched regions separated by 1 kb were merged and considered as blocks of variable lengths. All called peaks were then associated with genes by cross-referencing with the RefSeq TSS database. Peaks from individual experiments were considered overlapping if their peak centers were located within 200 bp. The peaks within 6 kb apart from the RefSeq gene TSS site were considered to be promoter bound. Enhancers were defined as \pm 1000 bp regions relative from the center of H3K27ac peak accumulation beyond 6 kb of an annotated RefSeq gene TSS. Genome browser tracks show tags or reads normalized to a sequencing depth of 10^7 reads.

Pearson Coefficient Correlation of histone marks

For the analysis shown in Figure 2A, we normalized tag counts in 2 kb windows around the peak center for each of the n = 55,113 annotated genomic regions with at least one histone mark (either H3K4me2, H3K27ac, or H3K4me3, or a combination of them, integrating our four experimental conditions). We used cor() command in R for calculating the similarities by Pearson Coefficient Correlation (PCC) (<https://www.rdocumentation.org/packages/stats/versions/3.6.1/topics/cor>). PCC scores were represented in a matrix heatmap.

Clustering of chromatin profiles

Using HOMER (RRID:SCR_010881), we identified n = 55,113 genomic regions with normalized tag enrichment of H3K4me2, H3K27ac, or H3K4me3 or a combination of them, integrating our four experimental conditions. Twelve-peak finding results were merged by using “mergePeaks” commands from HOMER with distance 1000 bp apart from the center of peak (“mergePeaks -d 1000 1.txt 2.txt 3.txt 4.txt 5.txt 6.txt 7.txt 8.txt 9.txt 10.txt 11.txt 12.txt -prefix com -venn plot_summary.txt -matrix statistics,” 1.txt –12.txt: denote for peak finding results from 12 different conditions). Peaks under each condition from “mergePeaks” results were concatenated as union peaks across the n = 55,113 enriched genomic regions. These regions were classified into k = 28 clusters using KMC: K-Means/K-Medians Clustering algorithm MeV_4_5 (<http://home.cc.umanitoba.ca/~psgndb/birchomedir/doc/MeV/manual/KMC.html>) based on the combinatory log scaled and normalized tag enrichment of the three histone marks and four experimental conditions. Mean for each cluster’s centroid vector was calculated and Pearson correlation was used as distance metric. 1000 was set as maximal iteration time. We used 6 kb windows around the center of each region, shown in the ChIP-seq heatmap. FOM: Figures of Merit from MeV_4_5 (<http://home.cc.umanitoba.ca/~psgndb/birchomedir/doc/MeV/manual/FOM.html>) was used to decide k = 28 as the input cluster number in KMC analysis, whereas the Mean adjusted FOM value get converged. Ten was used as FOM iteration number and 1000 was set as Max KMC iterations. For clarity, we re-annotated the 28 clusters, yet they were initially annotated by the algorithm. The 14 clusters with obvious changes in at least one condition were annotated as ‘variable’ clusters or patterns and the 14 clusters without obvious changes were annotated as ‘fixed’ clusters or patterns. The variable pattern with similar cisplatin response in A2780 and A2780cis cells was re-annotated as ‘P/S1’. The variable patterns with features characteristic of A2780 cells were re-annotated as ‘P2-P5’. The variable patterns with features characteristic of A2780cis cells were re-annotated as ‘R2-R10’. The re-annotation is the following: cluster1-> F1, cluster2-> F11, cluster3-> F2, cluster4-> F3, cluster5-> R10, cluster6-> F7, cluster7-> P4, cluster8-> F8, cluster9-> F5, cluster10-> P3, cluster11-> P5, cluster12-> F6, cluster13-> F4, cluster14-> F14, cluster15-> R6, cluster16-> F12, cluster17-> R2, cluster18-> R4, cluster19-> R8, cluster20-> F9, cluster21-> R7, cluster22-> F10, cluster23-> P/R1, cluster24-> R3, cluster25-> P2, cluster26-> R5, cluster27-> F13, and cluster28-> R9.

Similarity analyses of proximities and distances

The similarity analysis of distance of any two clusters' proximities (shown in [Figure 2E](#)) was defined by the sum of any two peaks' distances from compared two clusters and the distance was calculated and demonstrated by two-dimensional PCA analysis. Cluster/pattern proximities were defined by peak overlapping frequency between them, and the similarity distance was calculated and demonstrated by two-dimensional PCA analysis. First, any two clusters' peak distances were calculated using 200 kb as cutoff of distance between peaks, considered as 'overlap'. The raw counts of overlapping peaks were output in "statistics.count.matrix.txt" file. Second, the frequencies of overlapped peaks in a matrix were calculated through dividing the row of matrix from the output of "statistics.count.matrix.txt" by the total number of peaks in each cluster individually. Third, the PCA analysis was generated using HOMER (<http://homer.ucsd.edu/homer/basicTutorial/clustering.html>; RRID:SCR_010881) and using frequencies of overlapped peaks matrix as input. For the similarity analysis of distances (shown in [Figure 2F](#)), the peak distances compared between clusters were calculated by using mergePeaks commands in HOMER ('e.g. mergePeaks -d 10000 10.bed 11.bed 12.bed 13.bed 14.bed 15.bed 16.bed 17.bed 18.bed 19.bed 1.bed 20.bed 21.bed 22.bed 23.bed 24.bed 25.bed 26.bed 27.bed 28.bed 2.bed 3.bed 4.bed 5.bed 6.bed 7.bed 8.bed 9.bed -prefix k10 -venn k10_summary.txt -matrix k10-statistics', -d: distance between peaks which will be considered as overlap cutoff.). Natural log P-values for overlap using the hypergeometric distribution was used for Peak Co-Occurrence Statistics and showed by two dimensional heatmap (e.g., output file of 'k10-statistics.logPValue.matrix.txt' by 'mergePeaks'). And the effective size of the genome was selected as 2×10^9 . The Maximum distance between peak centers to merge were applied by 10 kb and 25 kb separately.

Super-enhancer analysis by ROSE

To identify SEs, we first applied the ROSE algorithm (https://bitbucket.org/young_computation/rose; RRID:SCR_017390) ([Lovén et al., 2013](#); [Whyte et al., 2013](#)). Briefly, MACS-identified peaks were stitched if they were within 12.5 kb of each other, and stitched enhancers were ranked by their difference in H3K27ac signal (density * length) versus input signal. A threshold separating super-enhancers from typical enhancers was identified by finding the point at which the line $y = x$ was tangent to a curve formed by plotting stitched enhancer rank versus H3K27ac signal – input signal. We ran the software using the additional option -t 2000, to exclude peaks fully contained within ± 2000 bases of an annotated promoter from stitching. Cutoff used: 452.3028, SE identified: 372 (A2780 vehicle, R#1), Cutoff used: 807.4458, SE identified: 341 (A2780 vehicle R#2), Cutoff used: 7056.1935, SE identified: 153 (A2780 drug R#1), Cutoff used: 2634.639, SE identified: 100 (A2780 drug R#2), Cutoff used: 5314.097, SE identified: 285 (A2780cis vehicle), Cutoff used: 8640.7872, SE identified: 415 (A2780cis drug).

PageRank motif analysis

We used PageRank (<https://github.com/kaizhang/Taiji>) to predict the most significant motifs enriched on regions enriched in H3K27ac or H3K4me2 and weighted by GRO-seq data. The effective genome size used was $1.87e+09$, band width was set as 300, and qvalue cutoff was set as 0.1. Model fold was ranged between 5 to 50. And 10kb windows were selected for calculating regional lambda.

HOMER motif analysis

We used algorithms described in HOMER (RRID:SCR_010881) ([Heinz et al., 2010](#)). The regions for *de novo* motif analysis was performed on sequences ± 500 bp relative to the peak center. Sequence logos were plotted by using WebLOGO (RRID:SCR_010236). Commands used ('findMotifsGenome.pl '+'peakfile+' 'hg18 genome'+'peakAnalysis_outputfolder'+ '-size 1000 -len 8,9,10,11,12,13,14,15 -S 50'), and detection motif length were screened from 8 bp to 15 bp, and 50 was set as number of motifs to optimize.

Analysis of GRO-seq density around ChIP-seq peaks

Normalized RPKM values by conditions across the different window sized region apart from the center of the ChIP-seq peaks (50kb, 500kb, and 5Mb) were collected and plotted by Box-plot way. The command ('annotatePeaks.pl '+'peakfile+' '+species+' '-size '+peaksizes+' -d '+samplelist+' > '+resultfile') from HOMER was used. The Welch Two Sample t-Test statistics was applied in calculating significance of signaling enrichment difference among four conditions (vehicle-treated A2780, cisplatin-treated A2780, vehicle- treated A2780cis and cisplatin-treated A2780cis). Level of P-values indicated in the figures.

Gene ontology analysis

The gene ontology analysis was performed using DAVID Bioinformatics (RRID:SCR_001881). We used the Functional Annotation option, Gene List using REFSEQ_mRNA, and terms were selected from the Functional Annotation Chart. We performed this analysis with the full list of dispersed genes in the M10-14 modules in [Figure 1H](#), or with the list of dispersed genes in each of the five modules, separately, in [Figure S1H](#).

Western blotting and quantitative real-time PCR (qRT-PCR)

Western blot and qRT-PCR analyses were performed as previously ([Almenar-Queralt et al., 2013](#)).

Immunofluorescent imaging

In 4- and 8-Well Glass chamber slides, cells were fixed with 4% formaldehyde solution (Sigma-Aldrich, Cat#F8775) in PBS (GIBCO, Cat#10010023) for 10 minutes at room temperature, washed three times in PBS, and permeabilized with 0.25% Triton X-100 (Sigma-Aldrich, Cat#T8787) in PBS for 10 minutes at room temperature, washed again three times in PBS for 5 minutes each, and blocked with 5% BSA (Sigma-Aldrich, Cat#A7906), 0.1% Tween 20 (Sigma-Aldrich, Cat#P9416) in PBS for 30 minutes at room temperature. Cells were incubated with mouse ISL1 antibody (1:1,000 dilution, Cat#39.4D5 s, DHSB; RRID:AB_2314683) in 5% BSA, 0.1% Tween 20 in PBS for three hours at room temperature. After three washes with PBS of 5 minutes each, cells were stained with anti-mouse Alexa Fluor-488 donkey anti-mouse IgG (H+L, 1:1,000 dilution, Life Technologies, Cat#A21202; RRID:AB_141607) in 5% BSA, 0.1% Tween 20 in PBS for two hours at room temperature. Cells were washed again with PBS for 15 minutes each with the first wash containing DAPI (1:1,000 dilution; Sigma-Aldrich, Cat#D9542) for nuclei staining. After adding Vectorshield mounting media (Vector Laboratories, Cat#H-1000), cells were imaged on a fluorescence microscope (model: BZ-X710, Keyance) using 20x and 100x objectives, and images were analyzed with ImageJ 1.51 s (RRID:SCR_003070).

Fluorescence-activated cell sorting (FACS) analysis by flow cytometry

Cells were grown in 15cm plates as > 50% cells are lost during the application of the staining protocol in solution. Cells were dispersed to a single cell solution using 0.25% Trypsin-EDTA (GIBCO, Cat#25200056) and washed with PBS (GIBCO, Cat#10010023) before fixation with 4% paraformaldehyde (Electron Microscopy Sciences, Cat#15710) solution in PBS for 15 minutes at room temperature (1.5mL). Centrifugations during the application of this protocol were performed for 1 minute at 3,500 rpm. After fixation, cells were washed twice in PBS and permeabilized with 0.25% Triton X-100 (Sigma-Aldrich, Cat#T8787) in PBS for 15 minutes at room temperature (1.5mL). Cells were then washed three times in PBS, and blocked with 5% BSA (Sigma-Aldrich, Cat#A7906), 0.1% Tween 20 (Sigma-Aldrich, Cat#P9416) in PBS for 30 minutes at room temperature (1.5mL). Cells were afterward incubated with mouse ISL1 antibody (1:150 dilution, Cat#39.4D5 s, DHSB; RRID:AB_2314683) in 5% BSA, 0.1% Tween 20 in PBS for three hours at room temperature (1.5mL). After washing twice with PBS, cells were stained with anti-mouse Alexa Fluor-488 donkey anti-mouse IgG (H+L, 1:1,000 dilution, Life Technologies, Cat#A21202, RRID:AB_141607) in 5% BSA, 0.1% Tween 20 in PBS for two hours at room temperature (1.0mL). After washing three times with PBS for at least 30 minutes in total, cells were resuspended in sorting buffer (2.5mM EDTA from Invitrogen, Cat#15575020, 25mM HEPES from GIBCO, Cat#15630080, and 1% BSA). In round-bottom, disposable, polystyrene tubes (Falcon, Cat#352235), cells were filtered and loaded onto the flow-cytometer instrument. FACS analysis was performed using the BD FACSAria™ Ilu flow cytometer using the FACSDiva Software (BD Biosciences; RRID:SCR_001456). Figures and quantifications were generated using the FlowJo 7.6.3 Software (OS version; RRID:SCR_008520). Experiments were performed 2-4 times monitoring 100,000 events per sample.

RNA-seq of fixed cells after FACS sorting

In order to separate low and high ISL1-expressing cells from a A2780 cell culture based on immunofluorescence detection of nuclear ISL1, we sorted 10 million fixed and stained A2780 cells, and gates were set with reference to negative (A2780-CRISPRi) and positive (A2780cis-CRISPRa) controls. We applied the same staining protocol described adding 1:100 RNasin Recombinant Inhibitor (Promega, Cat#N2515) to the fixation and permeabilization solutions and 1:25 RNasin Recombinant Inhibitor to the primary/secondary antibody solutions and the sorting solution. Six hundred thousand low ISL1- and high ISL1-expressing cells were collected in tubes pre-coated with a small amount of sorting buffer. After sorting, cells were pelleted and total RNA was isolated from the pellet using the RecoverAll Total Nucleic Acid Isolation kit (Thermo Fisher Scientific, Cat#AM1975), starting at the protease digestion stage of the manufacturer's protocols, as previously described ([Hrvatin et al., 2014](#)). Also as previously described ([Hrvatin et al., 2014](#)), instead of incubating cells for 15 minutes at 50°C and 15 minutes at 80°C, we carried out the incubation for 3 hours at 50°C and then frozen the samples at -80°C overnight before continuing the manufacturer's instructions. Isolated RNA was polyA-purified and converted to cDNA libraries using the TruSeq protocol (Illumina, Cat# 20020594) and AMPure XP beads (Beckman Coulter, Cat#A63881).

QUANTIFICATION AND STATISTICAL ANALYSIS

Software and tools used to perform statistical tests are explained in detail in every section. Error bars and biological repeats are indicated in the figure legends.

DATA AND CODE AVAILABILITY

All sequencing data generated in this study have been submitted to the NCBI Gene Expression Omnibus (GEO; <https://www.ncbi.nlm.nih.gov/geo/>) under accession number GSE129702.